AD-A174 553 RAPID SOLIDIFICATION PROCESSING AND POWDER METALLURGY OF AL ALLOYS(U) ILLINOIS UNIV AT URBANA DEPT OF MATERIALS SCIENCE H L FRASER 29 OCT 86 1/1

UNCLASSIFIED AFOSR-TR-86-1099 AFOSR-82-0186 F/G 11/6 NL

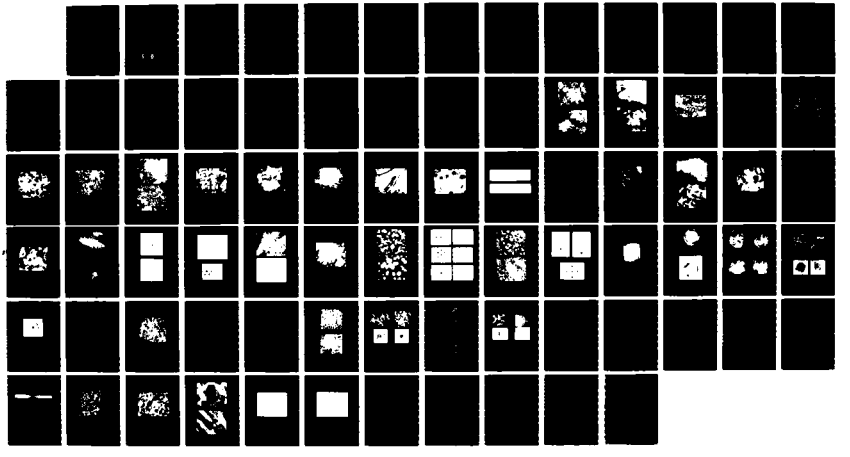

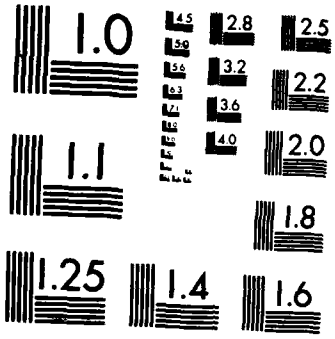

FINAL TECHNICAL REPORT

on

Rapid Solidification Processing and Powder Metallurgy of Al Alloys

AFOSR Grant No: AFOSR-82-0186

Submitted by

Hamish L. Fraser
Department of Materials Sciences
University of Illinois
1304 W. Green Street
Urbana, IL 61801

SECURITY CLASSIFICATION OF THIS PAGE

AD-A174 553

REPORT DOCUMENTATION PAGE

1a. REPORT SECURITY CLASSIFICATION: UNCLASSIFIED	1b. RESTRICTIVE MARKINGS
2a. SECURITY CLASSIFICATION AUTHORITY	3. DISTRIBUTION/AVAILABILITY OF REPORT: Approved for public release; distribution unlimited.
2b. DECLASSIFICATION/DOWNGRADING SCHEDULE	
4. PERFORMING ORGANIZATION REPORT NUMBER(S)	5. MONITORING ORGANIZATION REPORT NUMBER(S): AFOSR-TR- 86-1099
6a. NAME OF PERFORMING ORGANIZATION: University of Illinois; 6b. OFFICE SYMBOL (If applicable)	7a. NAME OF MONITORING ORGANIZATION: AFOSR
6c. ADDRESS (City, State and ZIP Code): 1304 W. Green Street, Urbana, Il 61801	7b. ADDRESS (City, State and ZIP Code): Bldg 410, Bolling AFB, DC 20332-6448
8a. NAME OF FUNDING/SPONSORING ORGANIZATION: AFOSR; 8b. OFFICE SYMBOL (If applicable): NE	9. PROCUREMENT INSTRUMENT IDENTIFICATION NUMBER: AFOSR-82-0186
8c. ADDRESS (City, State and ZIP Code): Bldg 410, Bolling AFB DC 20332-6448	10. SOURCE OF FUNDING NOS.

PROGRAM ELEMENT NO.	PROJECT NO.	TASK NO.	WORK UNIT NO.
~~2980~~ 61102F	~~[illegible]~~ 2306	A1	

11. TITLE (Include Security Classification): Rapid Solidification Processing and Powder Metallurgy of AL Alloys

12. PERSONAL AUTHOR(S): Hamish L. Fraser

13a. TYPE OF REPORT	13b. TIME COVERED	14. DATE OF REPORT (Yr., Mo., Day)	15. PAGE COUNT
FINAL	FROM 4/15/82 TO 4/15/86	Oct 29 86	75

16. SUPPLEMENTARY NOTATION

17. COSATI CODES			18. SUBJECT TERMS (Continue on reverse if necessary and identify by block number)
FIELD	GROUP	SUB. GR.	

19. ABSTRACT (Continue on reverse if necessary and identify by block number)

Regarding work on the development of microstructure during rapid solidification, three areas have been addressed. The first of these involved a determination of the mechanism of formation of the so-called zones A and B in hyper-eutectic AL-transition metal alloys. The second area of work involving the development of microstructure concerns submerged phase transformations. In a study of AL-Be hyper-eutectic alloys, it was determined that solidification proceeded by a set of phase transformations that may be described by a monotectic reaction. The third area of study concerning microstructural development involves quasi-crystalline AL alloys. In fact, work done in this program has concentrated on the potentially beneficial apsects of quasi-crystalline phases in the microstructure of AL alloys. Work on the consolidation of particulate has concentrated on the use of conventional techniques (i.e.extrusion)and novel processes (i.e. dynamic compaction). An estimate of the mechanical properties of rapidly solidified AL alloys has been obtained. As explained above, the effect of extrusion is to cause decomposition of the rapidly solidified microstructure. (over

20. DISTRIBUTION/AVAILABILITY OF ABSTRACT	21. ABSTRACT SECURITY CLASSIFICATION
UNCLASSIFIED/UNLIMITED ☒ SAME AS RPT. ☐ DTIC USERS ☐	UUUU

22a. NAME OF RESPONSIBLE INDIVIDUAL	22b. TELEPHONE NUMBER (Include Area Code)	22c. OFFICE SYMBOL
Alan Rosenstein	202-7674931	NE

DD FORM 1473, 83 APR EDITION OF 1 JAN 73 IS OBSOLETE.

SECURITY CLASSIFICATION OF THIS PAGE

INDEX

I. SUMMARY OF RESULTS

In this section of the final report, a brief outline of the main results obtained during the course of the work is given. Since the experiments performed may be conveniently placed into the various categories which make up the sections below, the results shall be discussed also in this way.

Regarding work on the ***development of microstructure*** during rapid solidification, three areas have been addressed. The first of these involved a *determination of the mechanism of formation of the so-called zones A and B in hyper-eutectic Al-transition metal alloys.* The mechanism for the formation of zone A involves undercooling the liquid alloy to a temperature that lies below that of the extended α-liquidus, so that it is possible for α-Al solid solutions to nucleate. The necessary degree of undercooling is achieved by the inhibition of the nucleation of equilibrium phases by the extremely rapid rates of cooling effected by rapid solidification processing (RSP). Continued growth of zone A microstructrues requires that recalescence from the liberation of latent heat of fusion is also inhibited by the rapid rate of heat extraction so that the temperature of the liquid at the solid/liquid interface does not increase above that corresponding to the extended α-liquidus. If the temperature does indeed rise above this value, then the solidification mode changes in that primary dendrites of an intermetallic phase may form, resulting in the formation of zone B. Zone B may also be formed directly if the cooling rate is not sufficient to produce the required degree of undercooling for the nucleation of either primary α-Al, or an eutectic mixture involving α-Al. This model for the formation of zone A has been used to explain the difference in the proportions of zone A present in Al-Fe-Mo alloys produced by atomization or melt-spinning. In the case of the former, while an high degree of undercooling may be achieved, the heat extraction coefficient is such that it is very difficult to inhibit recalescence in solidifying droplets. Therefore, generally the microstructures consist of a mixture of zones A and B, unless the powders are extremely small (typically less than ≈3μm). In contrast, the heat extraction coefficient in melt-spinning is much higher, and so recalescence may be inhibited more significantly, so that by maintaining the thickness of the ribbons less than ≈35μm, zone A microstructures may be obtained.

The second area of work involving the development of microstructure concerns *submerged phase transformations.* In a study of Al-Be hyper-eutectic alloys, it was determined that solidification proceeded by a set of phase transformations that may be described by a monotectic reaction. In fact, the shape of the equilibrium liquidus suggests that such a monotectic reaction is possible, providing that the equilibrium reactions involing an eutectic may be suppressed; this is achieved by rapid cooling. While it is apparent that an eutectic reaction may be suppressed by rapid

solidification, experiments done making use of Al-In alloys, where a monotectic reaction is exhibited in the equilibrium phase diagram, indicate that it is not possible to inhibit liquid phase separation that accompanies the pro-monotectic and monotectic reactions. Thus, it has been shown that rapid solidification of these alloys occurs by the equilibrium monotectic rather than by a metastable eutectic, as had been claimed previously in the literature.

The third area of study concerning microstructural development involves *quasi-crystalline Al alloys*. In fact, work done in this program has concentrated on the potentially beneficial aspects of quasi-crystalline phases in the microstructure of Al alloys. Thus, it has been shown for the first time that the second phase present in zone A of rapidly solidified Al-Fe alloys is in fact T′, a quasi-crystalline phase. This is modified to the icosahedral phase observed in rapidly solidified Al-Mn alloys, when V is added to the ternary Al-Fe-Mo. From hardness measurements at both room temperature and elevated temperatures and microstructural characterization, it has been concluded that the superior hardness (and strength) of zone A in Al-Fe based alloys when processed by RSP is due to the presence of a refined distribution of a quasi-crystalline phase in the microstructure. The decrease in strength when rapidly solidified Al-Fe alloys are annealed at temperatures ≈ 400°C is now attributed to the decomposition of the metastable quasi-crystalline phase. It has been noted that when Mo was added as a tertiary alloying element to Al-Fe alloys, that strength was maintained at an higher level during exposure at 400°C compared with the binary or other ternary alloys. Initially, this was thought to be due to the slow diffusivity of Mo in Al, but now it has been concluded that the rôle of Mo is to stabilize the quasi-crystalline phase itself.

Work on the ***consolidation of particulate*** has concentrated on the use of conventional techniques (i.e. extrusion) and novel processes (i.e. dynamic compaction). The *extrusion* of Al-8Fe-2Mo was performed at as slow a rate and as low a temperature as possble in an attempt to consolidate melt-spun ribbons possessing zone A without causing decomposition of the microstructure. This was not met with success, since the microstructure of the extruded material consisted of the products of decomposition of zone A. Experiments have been performed to show that the decomposition is due to adiabatic heating which accompanies the extrusion process. Thus, filaments of rapidly solidified Al-8Fe-2Mo were exposed at 400°C under the action of stress, below and above the yield stress for the material, and essentially no increase in decomposition rate was observed. The decomposition of the zone A microstructure may be avoided by the application of a consolidation technique where the sample is not subjected to a prolonged thermal exposure, such as *dynamic compaction*. Compacted samples of melt-spun Al-8Fe-2Mo consisting of zone A showed no indication of microstructural decomposition, and the as-rapidly solidified microstructure was preserved in the bulk form. While these compacts were extremely strong, they exhibited essentially zero ductility and further work is in progress aimed at improving this quantity.

An estimate of the ***mechanical properties*** of rapidly solidified Al alloys has been obtained. As explained above, the effect of extrusion is to cause decomposition of the rapidly solidified microstructure (i.e. of zone A). Consequently, a comparison has been made, using the alloy Al-8Fe-2Mo, between the tensile properties of the decomposed microstructure (i.e. extruded) and sub-scale test specimens produced by laser surface melting, consisting entirely of zone A. For example, the ultimate tensile strengths at room temperature are 462 and 520 MPa for the extruded and laser surface melted samples, respectively. At 315°C, this difference is much larger, being 282 and 401MPa, respectively. The superior strengths obtained for the zone A materials is attributed to the presence of the refined dispersion of the T′ quasi-crystalline phase in the microstructure. The fracture toughness of the extruded material has also been measured, and has been found to be ≈13.25MPa.√m in the T-L orientation. This is a disappointing result, and the low value of fracture toughness is attributed to the morphology of the intermetallic particles precipitated during decomposition of the rapidly solidified microstructure. These precipitates have needle-like shapes, which are not ideal for fracture toughness. Finally, the mechanical properties of some rapidly solidified Al-Be alloys have been determined.

2. INTRODUCTION

This report outlines the progress made in a three year study of the rapid solidification processing (RSP) of Al alloys. The study has involved work both in processing (both particulate production and consolidation), microstructural effects and mechanical properties. The aim has been to develop an understanding of the effect of various factors that influence rapidly solidified materials and so determine the mechanism of formation of microstructure. The microstructural modifications accompanying consolidation, using both conventional techniques employing prolonged thermal cycles and also a novel technique, viz. dynamic compaction, where consolidation avoids such thermal exposure, have also been investigated. Finally, the mechanical properties of the consolidated samples have been determined. In essence, the work has been aimed at developing an understanding of the effects of processing on the microstructure of Al alloys, using the measurement of mechanical properties to indicate where potential advantages with these materials and processing methods lie. The report begins with a summary overview of the background to rapid solidification of Al alloys, so that the work done in this program may be placed in an appropriate perspective.

The origin of the interest in RSP may be explained briefly. Of course, the properties of materials are influenced by microstructure, which in turn is influenced by processing. Thus, it is the modification of microstructure that is the basis of the potential advantages afforded by rapid solidification. The microstructure may be modified in one of four ways; firstly, RSP results in a marked increase in elemental homogeneity, which when taken together with the small size of particulate produced during rapid solidification implies that macrosegregation is eliminated. Secondly, supersaturated solid solutions may be produced directly from the melt; although these may find application at low temperatures, in the main they are intrinsically unstable and decompose during thermal exposures. However, extremely refined dispersions of second phase particles may be formed in this way; since relatively significant supersaturations of insoluble elements may be produced, the particles may be very stable against thermal excursions. Thirdly, while in many cases it may not be possible to achieve complete supersaturation, in general the microstructure of two phase materials is expected to be very refined. Finally, there is the possibility of producing metastable crystalline or amorphous phases.

These various methods of modifying microstructure have been applied to the case of *Al alloys*. In the main, improvements in the mechanical properties of these alloys have been sought; in particular, the elevated temperature tensile properties and fatigue resistance have been addressed. The reasons for this may be explained as follows. Firstly, precipitation hardening systems are

generally not suitable for elevated temperature applications because of the inherent instability of the strengthening particles against Ostwald Ripening [1]. For this reason, high temperature alloys contain a dispersion of more thermally stable particles; by employing conventional processing techniques, usually these cannot be dispersed on a sufficiently fine scale to effect optimum strengthening. Moreover, their relatively large sizes and shapes lead to inferior fatigue and fracture toughness responses. There is, therefore, an opportunity to employ rapid solidification in order to produce refined dispersions of thermally stable particles which may impart significant strength to these alloys. Also, in principle, it is possible that the presence of metastable phases, formed as a result of RSP, may also give rise to additional strengthening effects, and indeed it is shown below that this is the case.

Al alloys were used frequently in splat quenching experiments where studies were made not only of refined grain sizes, but also of the production of metastable phases [e.g. 2]. In general, these studies employed Al alloys in efforts to determine basic physical data concerning the microstructural modifications which are associated with rapid solidification. In contrast, the work of Jones [3] and Jacobs, Doggett and Stowell [4] was concerned with an investigation of possible enhancement of the properties of Al alloys at elevated temperatures that might be effected by rapid solidification processing. In the former study, Jones [3] noted that the contrast exhibited in optical micrographs of polished and etched samples of rapidly solidified Al-Fe alloys was either featureless or rather marked. These regions were termed "zone A" and "zone B", respectively. The hardness of zone A material was found to be significantly higher than that typical of zone B, and consequently much of the effort in terms of processing these types of alloy has been directed at the production of particulate possessing as large a fraction of zone A as possible.

Although RSP may offer some real possibilities for increases in elevated temperature properties, for Al alloys there are some disadvantages associated with this processing method. Thus, the nature of the technique means that particulate of some form is produced. This must be consolidated subsequently in some way. Al alloy powders are known to have adherent surface films consisting of hydrated oxides [5]; the presence of these layers gives rise to potential problems during compaction leading to a reduction in the level of bulk properties. This is an important consideration because the consolidation technique must be capable of providing sufficient shearing of the surfaces of the particulate to break-up the oxide layer and reveal clean metallic interfaces. Consequently, it may be predicted, and this in fact appears to be experimentally verified (see below), that it may be difficult to consolidate particulate of Al alloys in such a way as to reduce the associated thermal exposure and so preserve the as-rapidly solidified microstructure. However, the *full* exploitation of RSP in Al alloy development may only be realized if techniques of "cold" consolidation may be developed.

The remainder of the report is divided into three main parts. The first of these discusses the development of microstructures in rapidly solidified Al alloys. Then the compaction of particulate is considered, using both conventional and novel techniques. Finally, the mechanical properties of some rapidly solidified alloys are given, and these are related to the processing history and microstructures of the various samples.

3. DEVELOPMENT OF MICROSTRUCTURE

Rapid solidification involves a refinement of microstructure, and the production of extended solid solutions and metastable phases. In order to develop an understanding of the factors that are important in influencing the microstructure of alloys suitable for application, it was necessary first to develop an understanding of these factors in simple systems. For this reason, the rôles of undercooling and cooling rate have been assessed in the formation of the rapidly solidified microstructures (i.e. zones A and B) of *simple* Al-transition metal alloys. This has led to the developement of a simple explanation for these various microstructures which occur in these systems. Metastability has been shown to be significant in two alloy systems of interest, namely Al-Be and Al-Fe; in the former system, it has beeen shown that the equilibrium set of phase transformations that occur when conventionally processed is inhibited by rapid cooling such that solidification involves a metastable monotectic reaction. In the latter, it was found that the most significant strengthening component involves a refined dispersion of a metastable phase with the "quasi-crystalline" structure [6]. These various topics will be described below in turn.

3.1 Zone A and Zone B Microstructures in Hypereutectic Alloys

The nature and mechanism of formation of the so-called zone A and zone B microstructures in hypereutectic Al-transition metal alloys are of interest. These have been well-characterized in two simple systems, namely Al-Ni and Al-Co [7, 8 and 9]. In the case of Al-Ni alloys, there is a simple eutectic between α-Al and Al_3Ni, the eutectic composition being ≈3.05at.%Ni. Laser surface melting (CO_2 laser operating at between 3.5-5.0kW, scanned at ≈6.0cm.s^{-1}) has been employed to effect rapid solidification of Al-3.5Ni and Al-8.0Ni alloys (compositions in atomic %). Regarding the dilute alloy, only zone A microstructures were observed in optical micrographs of the re-melted regions. This microstructure has been characterized by transmission electron microscopy and is found in the main to consist of a cellular-dendritic morphology where the cross-sectional dimension of the cells is ≈0.2-0.5μm (Fig.1a). The inter-cellular precipitation is Al_3Ni. In some areas, a small amount of a micro-eutectic mixture of α-Al and Al_3Ni is formed, where the intermetallic compound is present in the form of rods (Fig.11b). The rod diameter is typically ≈20nm with the spacing between rods being ≈40nm. In the case of the Al-8.0Ni alloy, regions of both zone A and zone B were observed in optical micrographs taken from the re-melted regions. In the main, zone A consists of the micro-eutectic mixture (Fig.2a) described above, whereas occasionally there are regions of the cellular-dendritic microstructure

(Fig.2b). In marked contrast, the zone B microstructure consists of relatively coarse primary dendrites of Al_3Ni with α-Al at the interdenditic regions, as shown in Fig.3.

These various observations may be interpreted on the following basis. That part of the Al-Ni diagram containing the eutectic between α-Al and Al_3Ni is shown in Fig.4. Consider firstly the difference between the zone A and zone B microstructures observed in the Al-8.0Ni alloys. Zone A microstructures are either micro-eutectic or cellular-dendritic, based on α-Al. It seems reasonable to suppose that the liquid alloy has been undercooled during rapid solidification to a temperature somewhat below the extended α-Al liquidus, as indicated in Fig.4. At these temperatures, it is possible thermodynamically for α-Al to nucleate. Zone B consists of coarse intermetallic dendrites and corresponds then to a lower degree of undercooling with solidification occurring at a temperature above the extended α-Al liquidus. It is possible for zone B to form in one of two ways; firstly, the rate of heat extraction may be such as to undercool the liquid directly to a temperature above the extended liquidus.

Secondly, zone B microstructures may form as a result of recalescence; here, it may be assumed that sufficient undercooling is achieved so that solidification commences at a temperature below the extended liquidus, producing zone A microstructures. The formation of solid phases is accompanied by the liberation of latent heat of fusion which in an adiabatic system would result in an immediate increase in temperature. In the case where heat is being extracted at a rapid rate (i.e. as in a RSP process), this recalescence may be inhibited to a certain extent. If recalescence is such as to raise the temperature above the extended liquidus then the solidification mechanism will undergo a transition from the nucleation of primary α-Al (zone A) to primary intermetallic Al_3Ni (zone B). Consider now the different types of morphology for zone A, i.e. either cellular-dendritic or micro-eutectic. As depicted schematically in Fig.4, there is expected to be an asymmetry associated with the region of coupled growth, a situation typical of systems involving the growth of a faceted phase (in this case, the intermetallic compound) [10]. For the dilute alloy, the observed microstructure (cellular-dendritic) is consistent with an undercooling below the region of coupled growth. The relatively small amounts of micro-eutectic morphology observed in this alloy is then consistent with either a lesser degree of undercooling or to recalescence effects (i.e. a small rise in temperature). In the case of the Al-8.0Ni alloy, it appears that the liquid alloy is undercooled into the region of coupled growth; again, for a lesser degree of undercooling or a slight recalescence effect, the liquid temperature may be such as to correspond to dendritic growth. If this reasoning is correct, then an alloy of Al-6.0Ni when rapidly solidified should correspond to entirely zone A consisting of the micro-eutectic morphology. The result of such an experiment is shown in Fig.5, and it can be seen that only the micro-eutectic is present. *In summary, it appears that zone A microstructures form when the undercooling prior to nucleation is such as to reduce the temperature to below the extended α-Al lquidus, and the rate of heat extraction is such as to inhibit*

the effects of recalescence so that the liquid temperature does not rise above that liquidus.

The Al-Co system also contains a simple eutectic (at ≈2.0at.%Co) between α-Al and an intermetallic compound, in this case Al_9Co_2. Consequently, it would be expected that hypereutectic alloys would follow the same behavior as that described for Al-Ni. To establish this, samples of several alloys were laser surface melted, and the resulting microstructures characterized[9]. In all cases, the zone A microstructure of Al-3.5Co alloys was found to be cellular-dendritic (Fig.6), with a cell diameter of ≈0.2μm. For Al-5.0Co, this microstructure was mainly composed of a micro-eutectic mixture of the two phases (α-Al and Al_9Co_2), although some cellular morphology was evident, see Fig.7(a and b), whereas for Al-7.0Co both types of morphologies are present, Fig.8. It is clear that the trend in microstructural variation as a function of composition is essentially the same for these alloys as for Al-Ni. As stated above, zone B microstructures are expected to form either as a result of the effects of recalescence, or in situations where the undercooling is not sufficient to lower the temperature below the extended liquidus. An example of the latter is afforded by the case of laser surface melting of an Al-10.0Co alloy, where the undercooling necessary to produce zone A microstructures is large (≈300°C); all samples exhibited zone B microstructures, as can be seen from Fig.9, consisting of primary dendrites of Al_9Co_2.

An interesting result has been described by Garrett and Sanders [11] involving the melt-spinning of Al-Co hypereutectic alloys. In their work, large intermetallic particles have been observed, surrounded by a small region denuded of precipitation and then material exhibiting zone A morphology. These observations are inconsistent with the present model for formation of zone A since if these large particles were formed in the liquid during cooling, it is reasonable to expect that the recalescence associated with their growth would be sufficient to reduce the undercooling and so inhibit zone A formation. Similar melt-spinning experiments were repeated in an attempt to resolve this apparent controversy [9]. An example of one of these large particles in melt-spun Al-5.0Co is shown in Fig.10; an alternative explanation for their presence suggests that these particles are, in fact, unmelted primary intermetallic compounds. To ensure that all primary particles had been dissolved, the alloy was held for a prolonged period in the liquid state prior to melt-spinning. No such particles were then observed. If these large particles are indeed the remnants of primary dendrites from the as-cast alloy, then it needs to be established that during rapid cooling, these particles do not grow in size since otherwise recalescence effects would limit the achievable undercooling, thus inhibiting the formation o. zone A microstructures that are observed adjacent to these features. This is most readily done by examining the interface between melted regions and the underlying substrate in laser surface melted material. An example of this is shown in the optical micrograph in Fig.11 for the case of the Al-8.0Ni alloy; it is clear that large unmelted intermetallic particles are surrounded by zone A material, this being shown in more detail in the electron micrograph, Fig.12. The precipitate free zone about the particle is an indication that some regrowth

has occurred, but it is clear that zone A may form in the regions where large unmelted dendrites are situated. It is concluded that in areas where large particles exist which are surrounded by zone A material, it is most probable that these are unmelted dendrites.

In view of these various observations described above, it appears that two factors are important in influencing the formation of zone A microstructures. Firstly, it is necessary to cause the liquid alloy to be undercooled to a temperature below the extended α-Al liquidus. Of course, in principle, it is not necessary to employ rapid solidification to effect these high degrees of undercooling; thus, large undercoolings of bulk samples have been achieved by slow cooling (e.g.12,13). However, in a practical sense, powder metallurgy techniques involve many opportunities for heterogeneous nucleation, and so rapid cooling is extremely important for the development of large undercoolings prior to nucleation. Secondly, once nucleation has taken place, the growing nuclei liberate latent heat of fusion and it is necessary to effect a rapid rate of heat extraction to avoid the effects of recalescence which may cause the temperature to be increased above the extended α-Al liquidus. It is now possible to interpret the microstructures observed in rapidly solidified powders and compare these with those typical of melt-spun ribbons. An example of the microstructures of rapidly solidified powders of Al-8Fe-2Mo (wt.%) fabricated using the RSR process (centifugally atomized, forced convective cooling using He gas) are shown in Fig.13. As can be seen, most powders exhibit both zones A and B morphologies. These observations are rationalized as follows; during the forced convective cooling, a large degree of undercooling (below the extended α-Al liquidus) is achieved prior to nucleation such that zone A microstructures form. During further solidification, latent heat of fusion is liberated; the heat transfer coefficient is relatively small ($\approx 10^3 Wm^{-2}K^{-1}$, depending on droplet diameter (14)), and so the rate of heat extraction does not appear to be such as to inhibit recalescence sufficiently to avoid the temperature rising above the extended liquidus and therefore the formation of zone B. Only the smallest droplets will have very rapid heat transfer coefficients which may prove to be effective in inhibiting recalescence and result in powders whose microstructures may be described as entirely zone A. In marked contrast, the effective heat transfer coefficient for melt-spinning ($\geq 10^5 Wm^{-2}K^{-1}$)is significantly higher than that corresponding to powders and so it is possible to cast melt-spun ribbon consisting entirely of zone A microstructures. An example is shown in Fig.14 for the alloy Al-8Fe-2Mo (wt.%) which was produced by spinning on a steel wheel with a surface velocity of $\approx 35 ms^{-1}$ into an He environment.

3.2 Submerged Phase Transformations

In describing the microstructures observed in hypereutectic Al-Ni and Al-Co alloys, rapid cooling appears to inhibit the pro-eutectic reaction so that either cellular-dendritic or micro-eutectic morphologies form. In some systems, a somewhat different behavior is observed in that

not only is the pro-eutectic reaction inhibited but also the eutectic reaction is replaced by a submerged set of phase transformations. For example, consider the Al-Be system which exhibits an eutectic reaction between α-Al and Be at ≈2.5at.%Be, as shown in the phase diagram in Fig.15. Melt-spun ribbons of Al-4.4Be, Al-5.8Be and Al-20Be (compositions in atomic %) were prepared [15]; the microstructures are shown in Fig.16 a,b, and c, respectively. As can be seen, for the most dilute of these alloys, the microstructure is cellular-dendritic with a refined distribution of Be particles at the intercellular boundaries. In the case of the Al-5.8Be alloy, the microstructure consists entirely of a refined dispersion of Be particles in the α-Al matrix, whereas for the more concentrated alloy a bimodal distribution of Be particles exists. It may be considered that the microstructures are consistent with the eutectic reaction; thus, the microstructure of the more dilute alloy would correspond to undercooling below the extended liquidus into a region of cellular growth (based on nucleation of α-Al). The microstructure of Al-5.8Be would then correspond to undercooling into the region of coupled growth (which would have to exhibit a marked asymmetry) and the presence of large Be particles in the microstructure of the Al-20Be alloy would imply that the pro-eutectic reaction had occured during cooling.

There are two drawbacks to this line of reasoning. Firstly, the dispersed particles in the microstructure corresponding to Al-5.8Be are randomly distributed; the spheroidizing of a rod eutectic would result in a linear array of particles [16]. Secondly, the shapes of the large particles in Fig.16c are not consistent with these being produced during the pro-eutectic reaction. Thus, dendrites of primary Be in chill-cast material have a rather different, somewhat more conventional morphology. This may be emphasized by the micrograph shown in Fig.17, where it appears that these large Be particles form by coalescence. In fact, these observations are consistent with the refined dispersion of Be particles being produced by a monotectic reaction and the large Be particles forming as a result of a liquid phase miscibility gap. This suggested set of submerged reactions are also consistent with theoretical predictions. Thus, the slope of the Be liquidus is of interest since there is a point of inflection at ≈60-70at.%Be. Such curvature suggests the possibility of a submerged monotectic with an associated liquid miscibility gap [17]. It is tempting to speculate that the refined distribution of particles observed in the case of the Al-5.8Be alloy is produced by coupled growth associated with the monotectic reaction, while the large Be particles are a result of liquid immiscibility. A metastable phase diagram has been calculated to account for such a set of phase transformations, and is shown in Fig.18a [18]. The diagram is calculated as follows; firstly, on the basis of observation, the monotectic point is chosen to be ≈5.8Be. Secondly, the monotectic temperature is estimated by extending the equilibrium α-Al liquidus to the assumed monotectic composition. Thirdly, the miscibility gap and spinodal curves are calculated on the basis of the free energy for the equilibrium liquidus [19]. The Al-rich portion of the diagram is shown in more detail in Fig.18b; in this diagram, the shaded region corresponds to the region of coupled growth. In terms of this latter diagram, the microstructure of the Al-4.4Be alloy forms as a result of

undercooling into the region where α-Al forms in a cellular fashion; the composition of the remaining liquid changes such that it is in the region of coupled growth, resulting in the formation of a dispersion of particles in the intercellular boundaries (Fig.16a). The Al-5.8Be corresponds to the monotectic composition, and so solidifies in the region of coupled growth. Finally, the microstructure of the Al-20Be alloy corresponds to undercooling to a temperature approximately near to region 1 (Fig.18b) so that the reaction $L \rightarrow L_1 + L_2$ occurs; further undercooling causes the composition of L_1 to cross into the region of coupled growth, resulting in a refined dispersion of Be particles.

The diagrams shown in Fig.18 are a result of calculation and appear to fit the data well. For example, if an Al-4.4Be alloy were to be undercooled more significantly than has occurred apparently in the case of Fig.16a, it should be possible to effect solidification within the region of coupled growth. In fact, this is observed, Fig.19, in this alloy when observations are made in the electron transparent parts of melt-spun ribbons, i.e. regions which have experienced extremely rapid rates of heat extraction. However, the author, having an healthy disrespect for calculations, would point out that the positions of the metastable phase boundaries in Fig.18 should be more appropriately taken to represent approximations. It is not surprising, therefore, that refined distributions of Be particles have been observed to form in splat-quenched alloys containing very dilute concentrations of Be [20]. In terms of the present arguments, such observations are consistent with the production of an high degree of undercooling prior to nucleation and a slight 'shift' (to lower Be concentrations) in the position of the boundary between $\alpha+L_2$(cellular) and $\alpha+L_2$(coupled growth), Fig.18b.

The results described above refer to the case of melt-spun ribbons. The Be particles observed in these ribbons have been identified largely by diffraction studies, and are found to have the *hcp* crystal structure. In the case of laser surface melting (LSM), the rate of heat extraction is extremely rapid for Al alloys (because of the combination of an infinite heat transfer coefficient and a large value for the coefficient of thermal conductivity) and so an high degree of kinetic undercooling may be achieved. The microstructures of Al-Be alloys processed in this way (LSM) are similar to those described above for the case of melt-spinning, but the Be particles are found to possess the *bcc* crystal structure. Thus, Fig.20 shows micrographs of Al-5.8Be (a and b) and Al-11Be (c and d) alloys that have been rapidly solidified using LSM. As can be seen, the microstructure is produced by cooperative growth, even though in the case of the Al-11Be samples, there are large unmelted particles of Be present in the laser surface melted regions. Microdiffraction patterns obtained from particles in the same grain are shown in Fig.21; the diffraction maxima corresponding to the particles can be interpreted only on the basis of a *bcc* structure, and it is concluded that these particles represent a metastable form of Be. In addition to the microstructures consisting of a random distribution of Be particles in an Al matrix, in the proximity of large

unmelted particles (i.e. in the Al-11Be alloy) there exist rod-like morphologies, as shown in Fig.22a. A diffraction pattern obtained from one of these rods is shown in Fig.22b, and it has been simulated by the computer on the basis of *hcp* Be (Fig.22c), with an orientation relationship corresponding to $[101]_{Al}$ // $[0001]_{Be}$, and $(111)_{Al}$ // $(1210)_{Be}$. It is evident that both types of Be, viz. the equilibrium form (*hcp*) and a metastable phase (*bcc*), are observed to form during rapid solidification.

An explanation for this has been developed and involves the effects of recalescence that accompanies rapid solidification. Thus, it has been observed that the microstructures of the Al-Be alloys exhibiting cooperative growth have been processed by both LSM and melt-spinning. Therefore, it seems reasonable to assume that similar degrees of undercooling have been achieved during both types of processing, and so it is tempting to speculate that initially in both types of samples the Be particles have the *bcc* crystal structure. The effects of recalescence are more inhibited in the case of LSM than with melt-spinning because of the rapid rate of heat extraction provided by the combination of an infinite heat transfer coefficient and a large value for the coefficient of thermal conductivity in the case of the former. Therefore, during continued solidification in melt-spinning, the temperature of the soild will rise somewhat and this appears to be sufficient to cause the metastable form of Be to transform to the stable *hcp* structure. As noted above (Fig.22) in the Al-11Be alloy, Be particles with the *hcp* crystal structure were observed near to large unmelted Be; these large particles of unmelted Be are usually found in the region of the interface between the laser melted material and the underlying substrate. This region corresponds to solidification at a lower degree of undercooling because of the slow velocity of the solid/liquid interface during the initial period of regrowth, and so equilibrium Be forms; as the interface velocity increases, a significant kinetic undercooling develops and a transformation to the metastable form of Be occurs. The rods in Fig.22a breakdown to sherical particles as shown in Fig.23, indicating that the interfacial velocity has indeed increased, and diffraction studies performed on particles some distance from this breakdown show that the structure has changed from *hcp* (rods) to *bcc* (particles).

In an effort to increase the understanding of the metastable reactions involving submerged monotectic transformations, work was performed on Al-In alloys, where an equilibrium monotectic is exhibited. An interesting point concerning these alloys is that as a result of previous work performed by Ojha, et al. [21], it was concluded that solidification involved a metastable eutectic, a conclusion based on the presence of a metastable cubic In′ phase in the microstructure. Two types of rapidly solidified materials were used in this investigation, namely melt-spun ribbons and sub-micron powders produced by electro-hydrodynamic atomization, the latter being provided kindly by Dr.S.Ridder of the National Bureau of Standards. The microstructure observed in the melt-spun ribbons may be described as follows. In parts of the ribbon sufficiently thin for electron

microscopy without requiring thinning, there are some areas containing both large irregularly shaped particles of In (face-centered tetragonal (*fct*)) and smaller faceted particles (Fig.24), and other regions exhibiting refined dispersions of the small faceted phase, Fig. 25. Computer simulation of diffractions patterns recorded from the faceted particles are consistent with the In′ (*fcc*) phase (see Fig. 26). In ribbons thinned by ion-milling, a bimodal distribution of faceted particles is observed (Fig.27), and these have been shown to be In′. An interesting observation involves streaking of the diffraction maxima originating from the precipitates, an example being shown in Fig. 28. The large particles, apart from being faceted, exhibit Moiré fringes (Fig.29); these Moiré fringes are somewhat 'wavy', an explanation for this being given below.

These various observations may be interpreted on the basis of the monotectic reaction exhibited in the equilibrium phase diagram. Thus, the presence of both large and small particles of In′ in the microstructure is consistent with the liquid phase separation produced during the pro-monotectic reaction and also the monotectic itself. If indeed a metastable eutectic reaction had occurred, the microstructure would be expected to consist of large regions of α-Al from the pro-eutectic reaction together with small regions of In (or In′) either intimately mixed with α–Al, or in an α-Al matrix, if, in the case of the latter, the eutectic α-Al forms in a divorced fashion. This type of microstructure is not observed, and it is concluded that the rapid solidifcation of this alloy involves the monotectic reaction indicated in the phase diagram.

The observation of both forms of In, namely In (*fct*) and In′ (*fcc*) is interesting; it is noted that in general the In′ forms when constrained by the α-Al matrix. This is most clearly shown in the in-situ remelting experiments performed with sub-micron particles produced by electro-hydrodynamic atomization. These powders, of composition 7.3 at.% In, were supported on a graphite film and intoduced into the electron microscope in an heating stage. Melting was effected by focussing the electron probe onto the given powder and subsequently rapidly solidified by deflecting the beam, in a manner described previously elsewhere [22]. The microstructure of the powders in the as-received condition consists of a small number of relatively large particles of In (*fct*) situated at the surface of the powder, and a fine dispersion of In′ in a matrix of α-Al, as shown in Fig.30. The diffraction information supplied with Fig.30 shows the diffraction maximum from the In′ particles aligned parallel to the 111 systematic row of α-Al, and two maxima from the large In (*fct*) particles, shorter in length and slightly misaligned with respect to this systematic row. The In′ particles exhibit faceted shapes, which have been determined to be octahedra with facets parallel to {111} in α-Al, truncated by {100}. The heating stage has been used to vary the temperature of the powders in order to determine the thermal stability of the In′ phase. As can be seen in Fig.31, the particles remain facetted, even when the In′ has melted, up to a temperature of ≈ 523K. Upon cooling and resolidifying, the In′ crystal structure still persists, even though the rate of cooling is relatively slow. Therefore, it is concluded that the rate of solidification has little affect

on the formation of the metastable phase In′ which appears to be influenced more significantly by the fact that solidification occurs within a faceted cavity.

Two interesting observations are evident; the first of these is that the cavities remain faceted in the presence of liquid In. The shape of such a cavity is determined by several factors, among which is the anisotropy of the surface energy. Since in pure Al this physical quantity is fairly isotropic, it is presumed that the presence of liquid In causes an anisotropy in the surface free energy to develop. The second observation involves the fact that when In droplets solidify in an Al-In alloy, those droplets that are unconstrained by the Al matrix form with the equilibrium structure, i.e. *fct*, whereas those that form within the α-Al matrix, particularly within a faceted cavity, form as In′. The occurrence of the In′ phase in the facetted particles may be rationalized by consideration of several factors. Firstly, Raynor and Graham [23] have determined that the tetragonality of In decreases with temperature. Their measurements were made at temperatures up to 408K, where the axial ratio was found to be given by c/a = 1.065. The tetragonality is also decreased by alloying with elements whose valencies are 3 or less [24-26]. It is reasonable to assume that, given the comined effects of temperature and alloying, the In in the cavities has formed directly as In′. In this case, the orientation relationship observed (cube-on-cube) is consistent with the sharing of symmetries between the two cubic structures. There is ≈ 13.8% misfit across adjacent {111} planes, and this would in principle give rise to both misfit dislocations and the nucleation of prismatic loops in the matrix in order to cause an effective relieving of this strain. However, the elastic modulus of In is ≈ ten times smaller in value than that of Al, and so it is possible to introduce misfit dislocations into the In′ without increasing the elastic energy of the system inhibitively. A simple calculation shows that a network of dislocations spaced ≈ 2.4nm apart would be sufficient to account for the misfit between the phases.

It should be possible to image the proposed dislocation array with techniques such as weak-beam dark-field microscopy, but several factors prevent this from being done. Thus, it is necessary to make observations on thin foils; when the In becomes exposed to laboratory air, i.e. when very thin foils are used, the phase oxidizes rapidly. Secondly, it has been estimated that the dislocations are very closely spaced (≈2.4nm) in a material with very low elastic modulus, and this makes imaging of the dislocations extremely difficult. Rather than present direct evidence for such a closely spaced array of dislocations, indirect observations may be used to support this supposition, i.e. that these dislocations are indeed present. Thus, it was noted above that the Moire′ fringes shown in Fig.29 are wavy and this is consistent with the presence of an array of dislocations. More significantly, streaking was observed in the diffraction maxima produced by the In′ phase, the streaks being parallel to <110> directions. It has been shown that streaks may be produced in a direction perpendicular to a dislocation line when that dislocation itself is perpendicular to the foil normal [27]. In the present case, an array of edge dislocations with **b**=1/2<110> would account for

the streaks associated with the 220 and 200 reflections of In′. Hence, it seems reasonable to conclude that an array of dislocations does indeed exist in the In′ to account for the lattice mismatch between matrix and second phase. As the temperature decreases, the In′ phase does not revert to the equilibrium form, and this is most probably attributed to the reduction in the elastic energy associated with the sharing of symmetries and the low energy nature of the interface produced by the presence of low energy misfit dislocations. Finally, it is interesting to note that the In forming from the pro-monotectic reaction at the surfaces of the powders is of the equilibrium form, i.e. *fct*. There are two possibilities concerning the solidification of this phase; firstly, as the In is unconstrained, it is likely that the equilibrium form nucleates at the α-Al/liquid In interface. Alternatively, it may be proposed that the In in these unconstrained particles does in fact nucleate first as In′ since sharing of symmetries may occur and low energy dislocations may be introduced to account for the lattice mismatch. On cooling to ambient temperatures, the metastable phase would then transform to the equilibrium form since it is not constrained in the same way as material contained in the cavities. Further work is currently in progress.

3.3 Quasi-Crystalline Al Alloys

During the course of the present study, rapid solidification of Al-Mn alloys was studied. In these alloys, rapid solidification is accompanied by the formation of phases now known as quasi-crystals [6]. Such phases exhibit five-fold selected area diffraction patterns, and have more recently been observed in several Al and other alloys [e.g. 28,29]. At least two different structure types have been identified [30]. The structure of these phases has been the subject of considerable discussion; the most notable theory is based on Penrose tiling [31], and has been developed by several workers [e.g. 32,33]. An alternative theory involves twinning, which was first proposed by Field and Fraser [34] *as a result of work performed in this program*, and more recently by Pauling [35]. The twinning model is not considered seriously because of several experimental facts, derived from high resolution electron microscopy, convergent beam electron diffraction and dark-field electron microscopy. However, perhaps the most clear evidence showing that the twinning model is inappropriate involves it's inability to account for the diffracted intensities in diffraction patterns corresponding to ***minor*** poles; it is certainly sufficient to account for the high order poles. Of course, it is necessary for any model to account for all of the reciprocal lattice, and this needs to be established for the more sophisticated models.

An important question concerning quasi-crystals in rapid solidification involves the potential usefulness of these phases in developing Al alloys with high temperature strength. Consider the alloys Al-8Fe-2Mo and Al-7.9Fe-2.9Ce (compositions in wt.%). (These alloy

compositions were chosen such that they correspond to 4.1at.%Fe, and 0.6at.% of either Mo or Ce). The zone A microstructures of laser surface melted samples of these alloys are shown in Fig.32a and b, respectively, while the selected area diffraction patterns are given in Fig.33a and b, respectively. The two microstructures are somewhat similar, being cellular-dendritic. At the intercellular regions there exists a randomly oriented, refined dispersion of a second phase, this being deduced from the presence of the concentric rings that are observed in the diffraction patterns. The cell sizes in the two alloys are approximately the same and the main difference in these two microstructures involves the scale of the intercellular precipitation, this being somewhat coarser in the case of the Ce containing alloy; this is most readily apparent from the less-diffuse nature of the diffraction rings in the pattern from this alloy (Fig.33b). It has not been possible to identify the intercellular precipitation from the data contained in the SAD patterns. Recently, however, the nature of the phase has been determined using convergent beam micro-diffraction [36]. An example of a pattern recorded from the Ce containing alloy is shown in Fig.34, and as can be seen, it exhibits the symmetry possessed by quasi-crystals. In fact, this and other patterns recorded from the same particle may be interpreted on the basis of the T′ phase [31]. The position and number of the rings in the two SAD patterns, Fig.33a and b, are essentially the same except for the fact that the more refined microstructure of the Mo containing alloy causes the weakly diffracting reflections of some of the rings to be too diffuse to be observed. Consequently, it has been concluded that the intercellular phase in both rapidly solidified alloys is T′.

The micro-hardnesses of the two alloys (Mo and Ce containing) as well as the ternary Al-9.2Fe have been measured as a function of isochronal annealing at 400°C, see Fig.35 [7]. Of particular interest are the values corresponding to the as-rapidly solidified condition (i.e. zero time); the binary and Mo containing alloy exhibit the highest hardness, whereas the Ce containing alloy has a significantly lower value. It is interesting to correlate this difference in hardness (and presumably strength) with microstructural features. Thus, the strength of these rapidly solidified alloys may be influenced by the cell size, the presence of supersaturated solid solutions and/or the refined distribution of intermetallic particles at the intercellular regions. In terms of the cell size, as stated above the cell sizes of the two ternary alloy are approximately the same, so that this factor cannot account for the difference in hardness. The compositions of the α-Al cells have been measured using energy dispersive x-ray analysis (EDS) combined with scanning transmission electron microscopy (STEM) [7] and the results are shown in Table 2. As can be seen, the alloys each exhibit a fairly high degree of supersaturation regarding solute elements, and it is difficult to attribute the difference in hardness to this factor. However, it has already been shown that the scale of the intercellular precipitation is significantly finer in the case of the Mo containing alloy compared to that in the Ce containing alloy. Indeed, the diffraction patterns from the binary alloy are essentially identical to the Mo containing alloy, and so it is concluded that *it is the presence of a refined dispersion of a quasi-crystalline phase that is important in effecting the strength of zone*

A microstructures. The importance of the quasi-crystalline phase is now evident, especially since the marked drop in hardness associated with annealing the binary alloy at 400°C is caused by decomposition of this phase, Fig.36. The quasi-crystalline phase appears to be stabilized by the presence of Mo and Ce, see below, and so the hardnesses of these alloys remains high with continued annealing at 400°C.

ALLOY	Al	Fe	Mo	Ce
	(composition in wt.%(at.%))			
Al-9.2Fe	bal	7.7(3.9)	---	---
Al-8.0Fe-2.0Mo	bal	3.8(2.1)	2.0(0.6)	---
Al-7.9Fe-2.9Ce	bal	6.1(3.1)	---	2.0(0.4)

Table 1. Chemical compositions of the α-Al cell interiors determined by EDS and STEM. Note that the compositions of the binary alloy in atomic % is 4.7Fe, while the ternaries correspond to 4.1Fe and 0.6% of either Mo or Ce. For example, the maximum equilibrium solid solubility of Fe in Al is ≈0.05wt.%.

It is interesting to compare the intercellular regions observed in the Al-Fe alloys with those observed in Al-Mn alloys. In the case of the latter, the icosahedral phase is formed at the intercellular regions, and SAD patterns recorded from this phase correspond to those equivalent to "single crystals". This difference in morphology may be explained by considering the mechanism of formation of the randomly oriented particles in the case of the Al-Fe alloys. It has been determined that the Al matrix is slightly supersaturated with in Fe, see Table 2. Therefore, after nucleation occurs, the intercellular regions consist of a highly undercooled liquid which is rich in Fe. It is tempting to speculate that as the liquid in the intercellular regions becomes enriched in Fe, at some particular composition for a given temperature, a glass transition occurs. It is possible during the slight recalescence that will occur even in systems that provide very rapid rates of heat extraction for this amorphous material in the intercellular regions to be heated above the "crystallization" temperature such that a quasi-crystalline structure is formed. Considerable indirect support for this model may be derived from the recent work of Urban, et al. [37]. In that study, thin foils of a rapidly solidified Al-Mn alloy containing the "single crystal" form of the icosahedral phase were electron irradiated so that an amorphous alloy was produced. On heating this glassy structure while irradiating the sample, a refined distribution of particles was formed, rather than the "single crystal" structure produced initially as a result of rapid solidification.

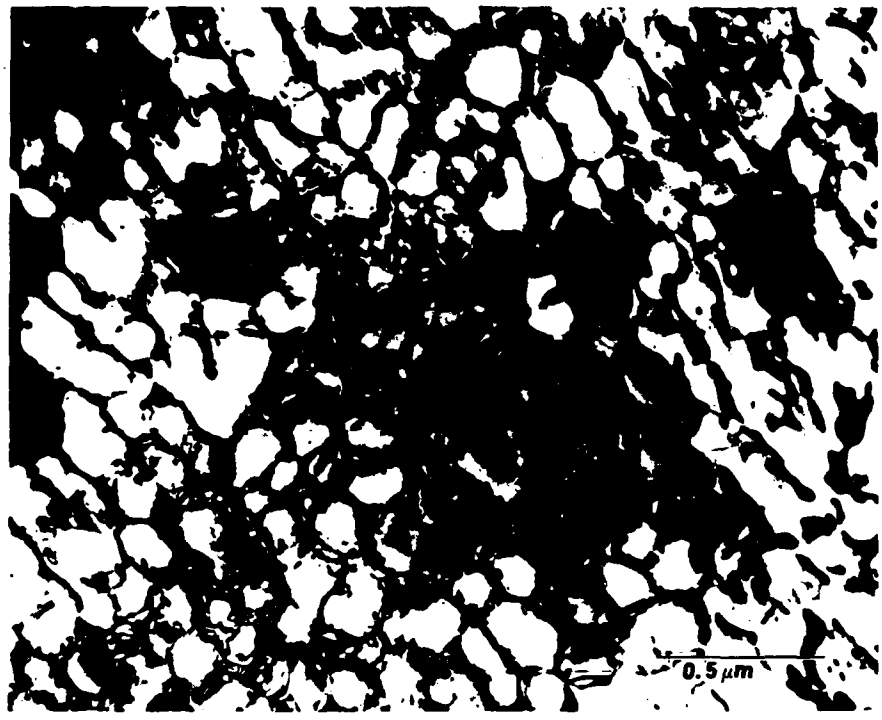

(a)

(b)

Fig.1. TEM micrographs of laser surface melted Al-Ni alloys: a) 3.5 at .%Ni zone A consisting of a cellular primary α–Al structure; b) 3.5 at.%Ni zone A exhibiting some micro-eutectic mixture and a cellular region.

(a)

(b)

Fig.2. TEM micrographs of laser surface melted Al-Ni alloys: a) 8.0 at.%Ni zone A showing the predominantly micro-eutectic structure; b) 8.0 at.%Ni zone A showing both micro-eutectic and cellular region.

Fig.3. TEM micrograph of an 8.0at.%Ni zone B region showing large primary dendrites of Al_3Ni intermetallic compound.

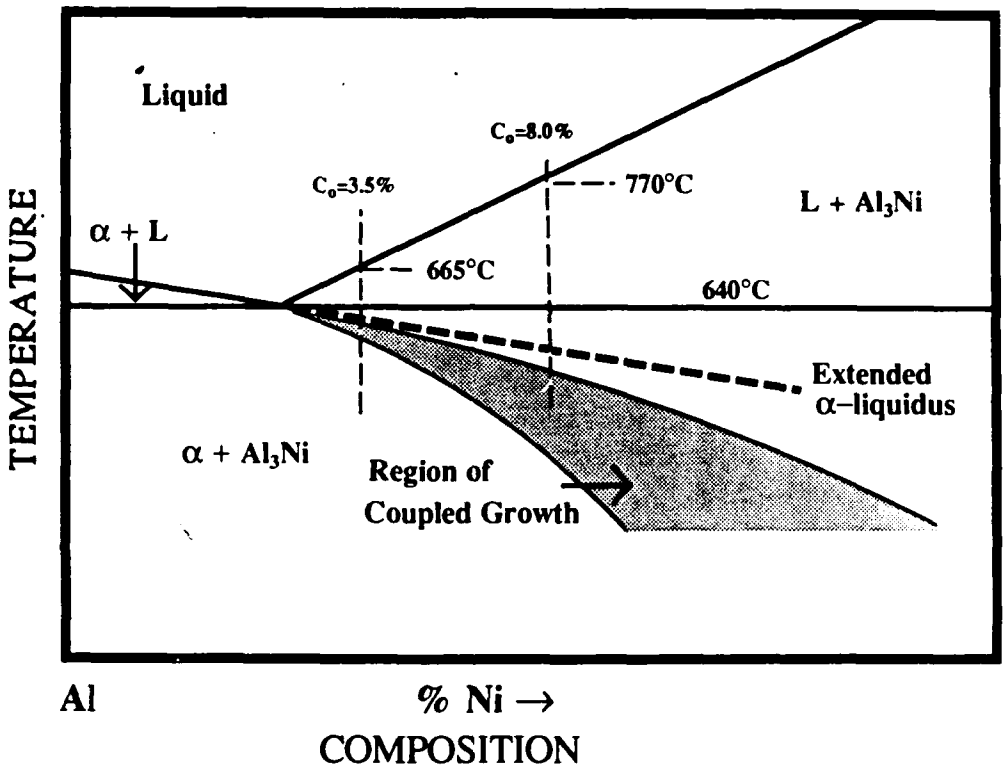

Fig.4. Phase diagram of the Al-rich part of the Al-Ni binary system. Also shown are the extended α–Al liquidus and asymmetric coupled growth region.

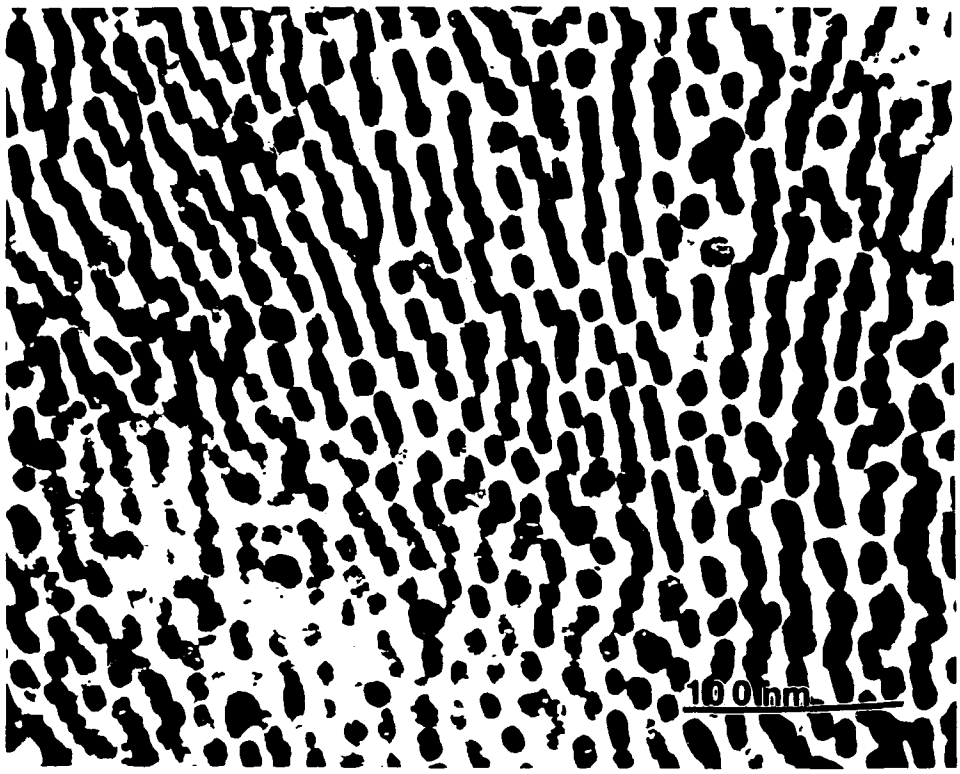

Fig.5. TEM micrograph of laser surface melted Al-6.0at.%Ni consisting only of the micro-eutectic morphology.

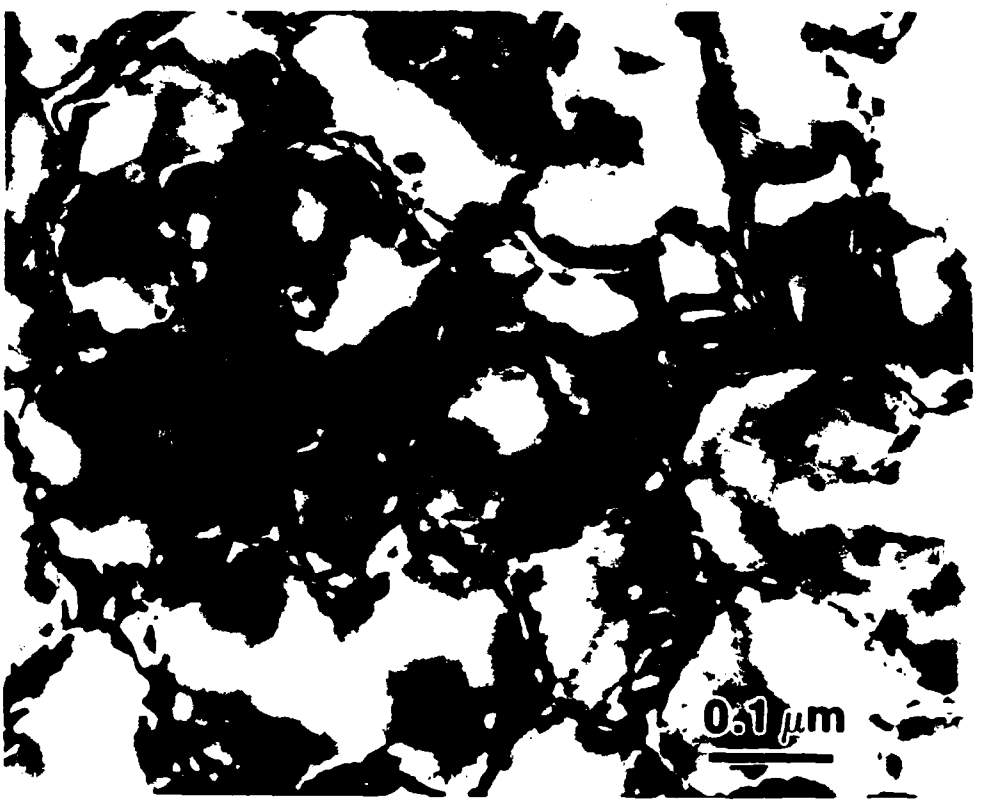

Fig.6. TEM micrograph of laser surface melted Al-3.5at. %Co. The microstructure appears to be micro-cellular, based on α–Al.

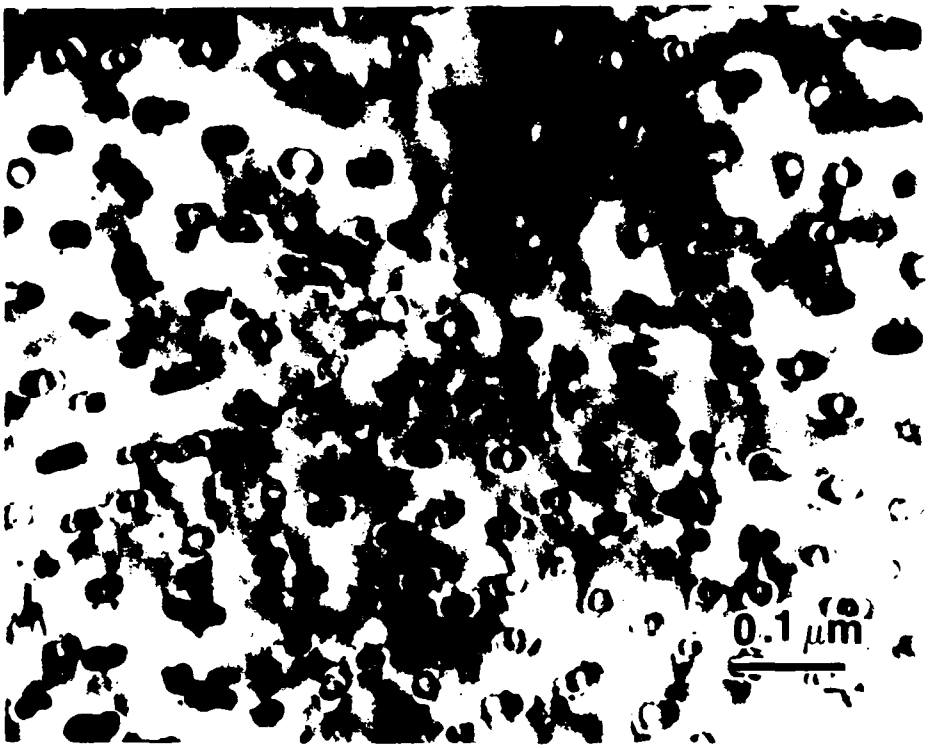

Fig.7. TEM micrographs of the micro-eutectic microstructures associated with laser surface melting of Al-5.0at. %Co.

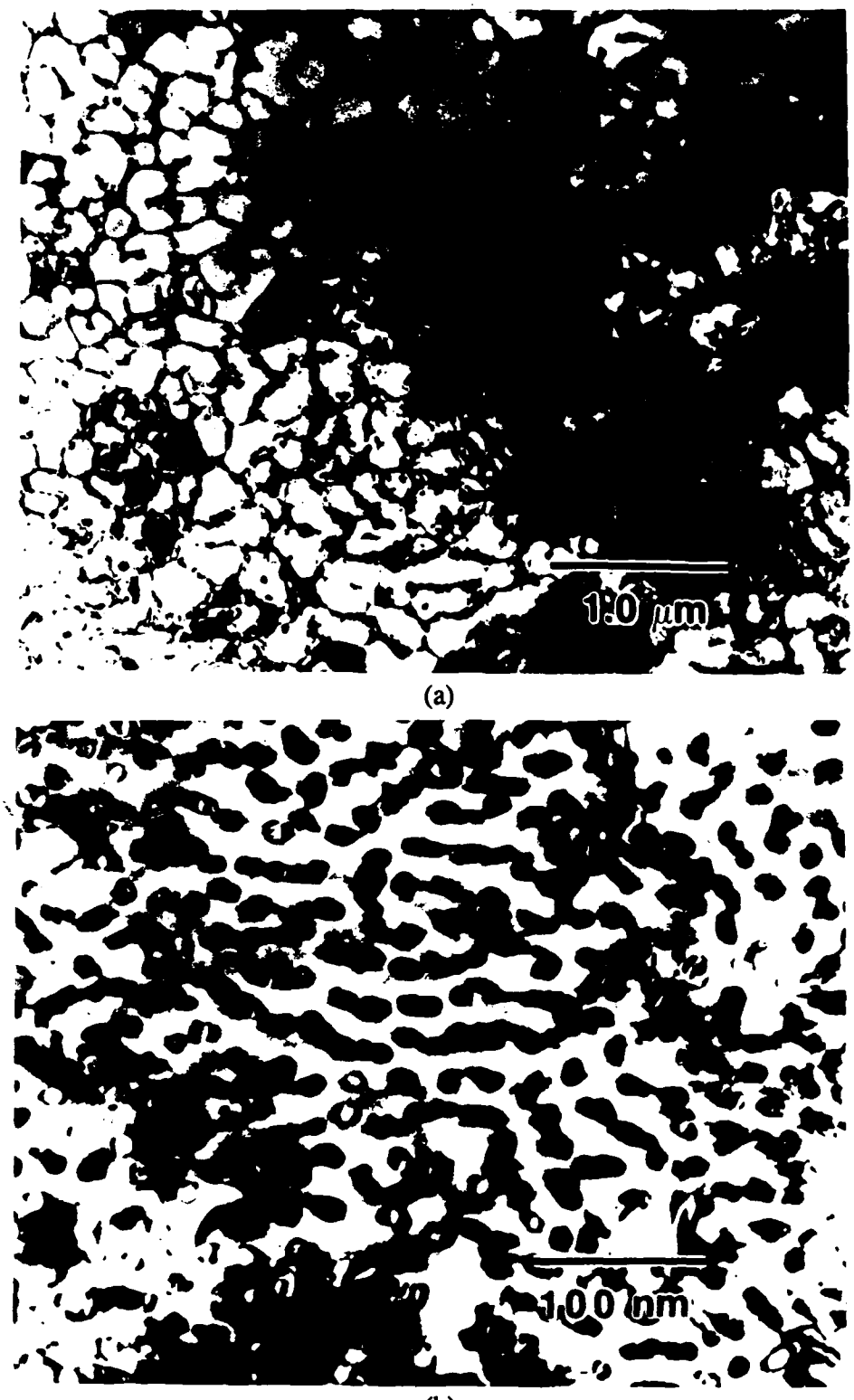

Fig.8. TEM micrographs showing the morhologies found in the microstructures of laser surface melted Al-7.0at. %Co alloys. a) microcellular; b) microeutectic.

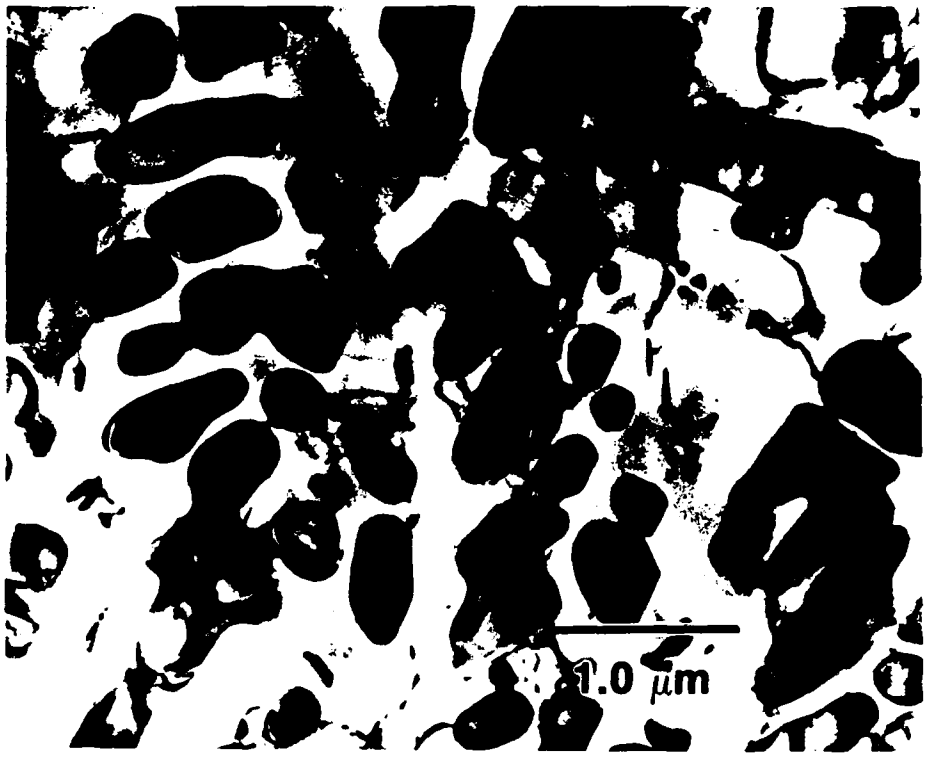

Fig.9. TEM micrograph showing the zone B microstructure associated with laser surface melted Al-10.0at. %Co.

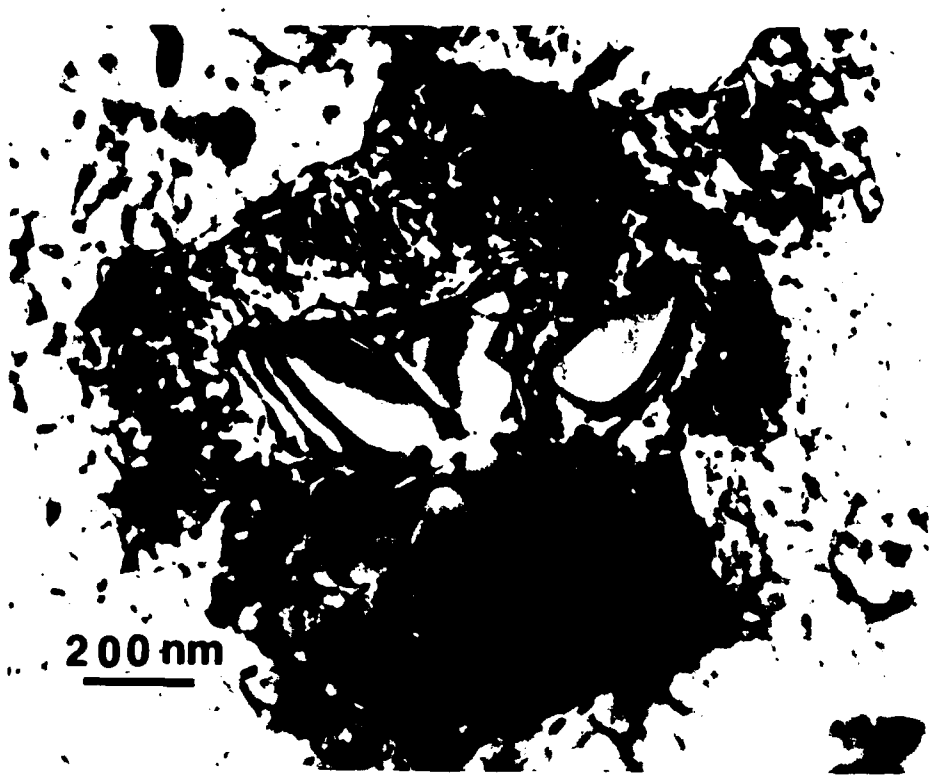

Fig.10. TEM micrograph of melt spun ribbon of Al-5.0at.%Co. A large stellated particle of Al_9CO_2 is present in the micrograph.

Fig.11. Optical micrograph of a transverse section of a laser surface melted Al-8.0at.%Ni from a region which was not completely melted.

Fig.12. TEM micrograph of an unmelted Al_3Ni intermetallic particle surrounded by the micro-eutectic mixture corresponding to zone A.

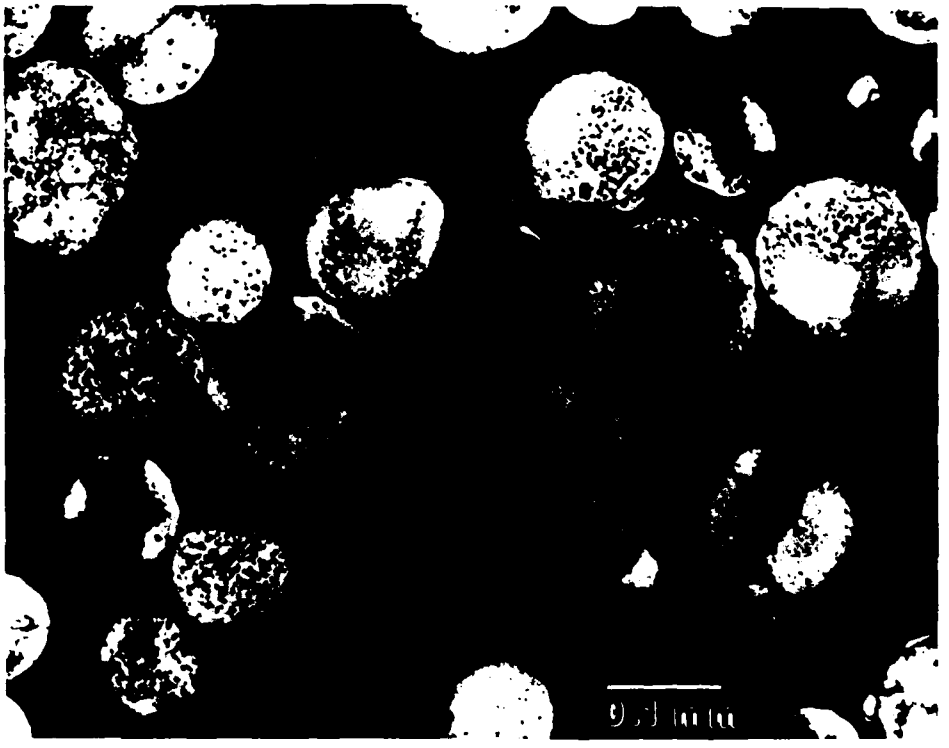

Fig.13. Optical micrograph of Al-8Fe-2Mo powders produced by the *RSR* process.

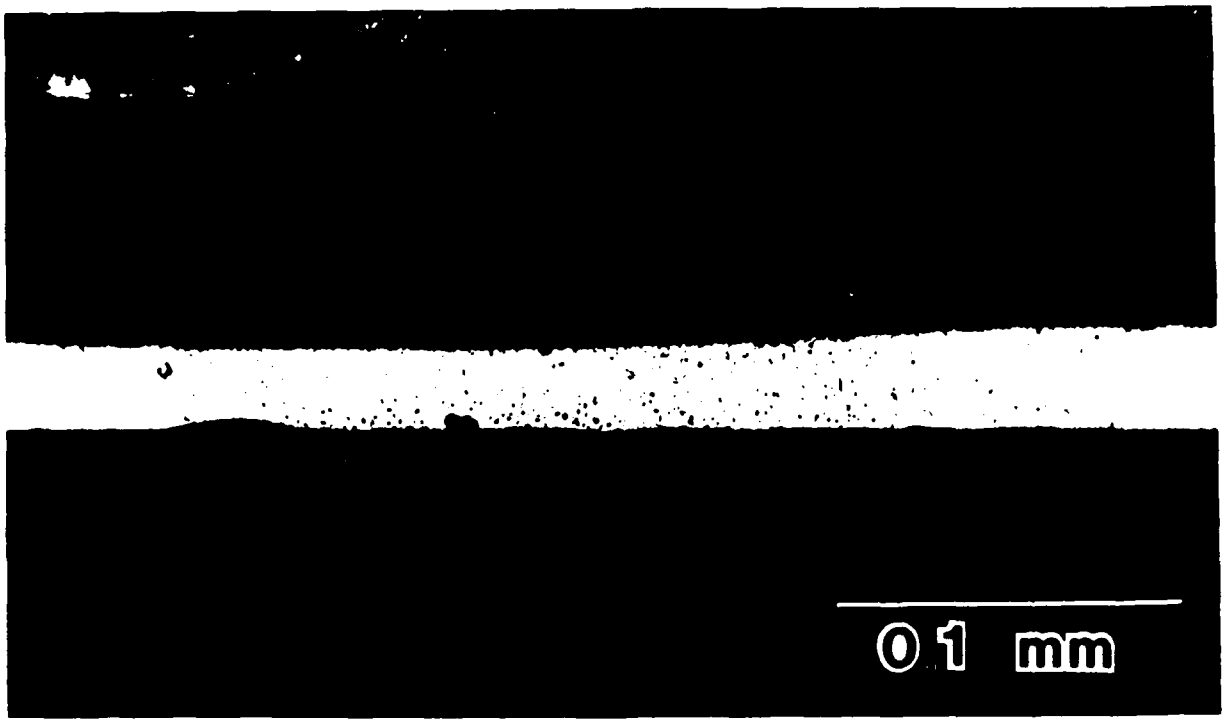

Fig.14. Optical micrograph of Al-8Fe-2Mo prepared by melt-spinning. See text for details.

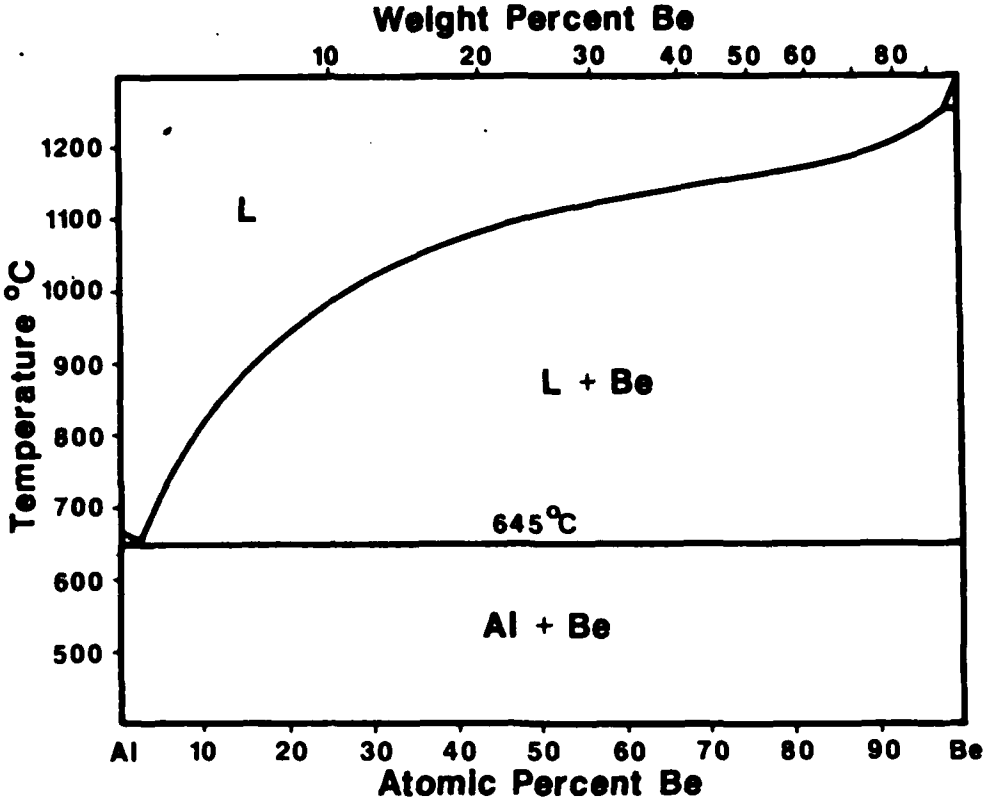

Fig.15. Al-Be equilibrium phase diagram.

(a)

Fig.16. (a) Bright field electron micrograph of the melt-spun Al-4.4 Be alloy. The grain observed consists of three subcells with intercellular precipitates. (b) Bright field electon micrograph of the melt-spun Al-5.8 Be ribbon. (c) Bright field electron micrographs of the Al-20.0 Be alloy. The large irregular shaped particles represent the prior pro-monotectic L_2 liquid.The finer precipitates are produced during the monotectic reaction.

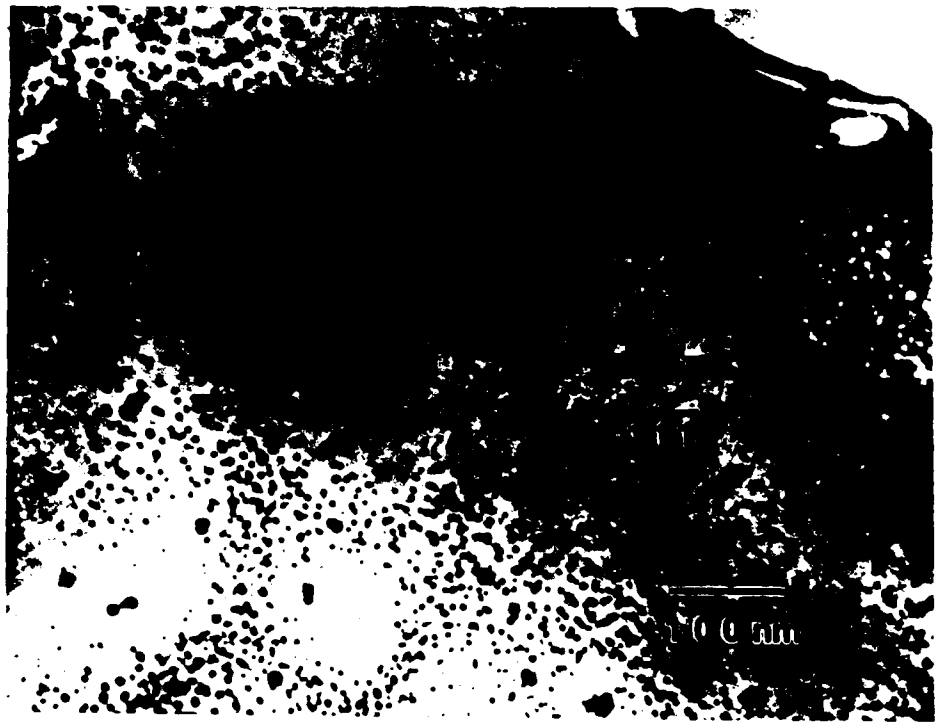

(b)

(c)

Figure 16 - continued

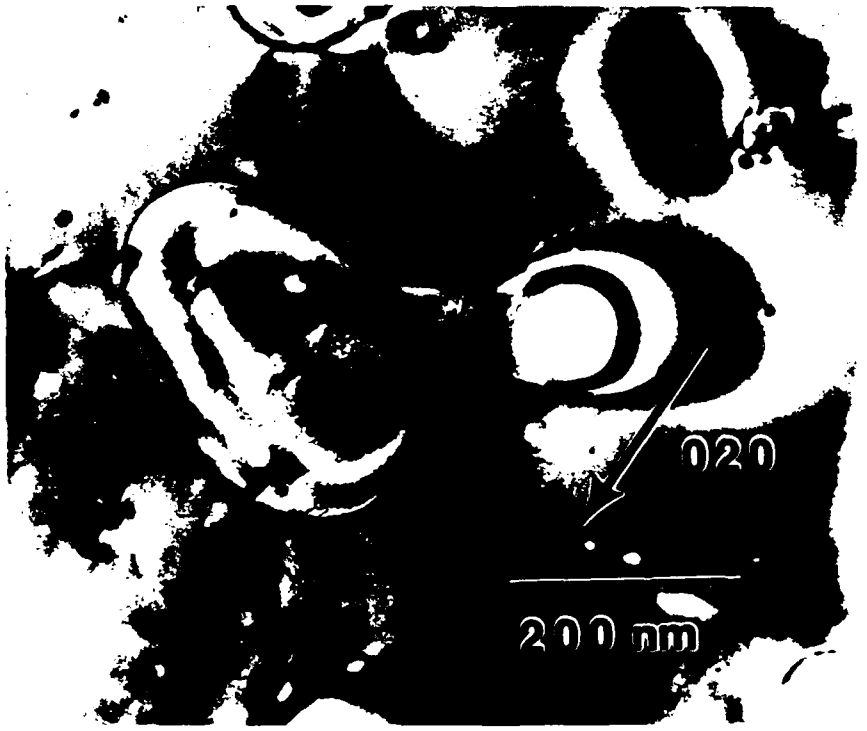

Fig.17. Bright field electron micrograph showing the coalescence of the pro-monotectic L_2 phase in the Al-20.0 Be alloy.

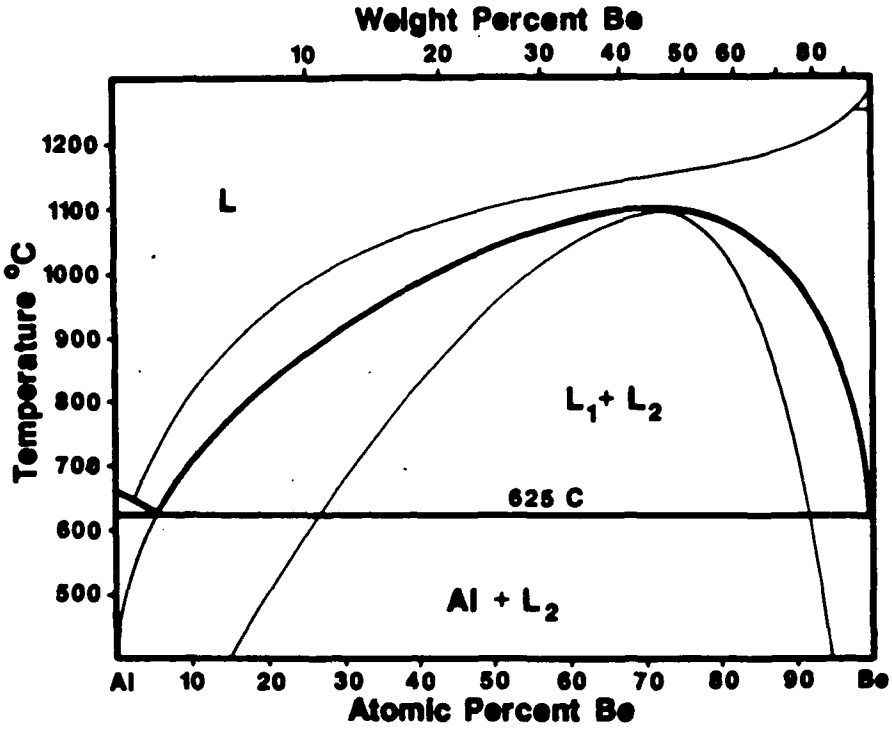

(a)

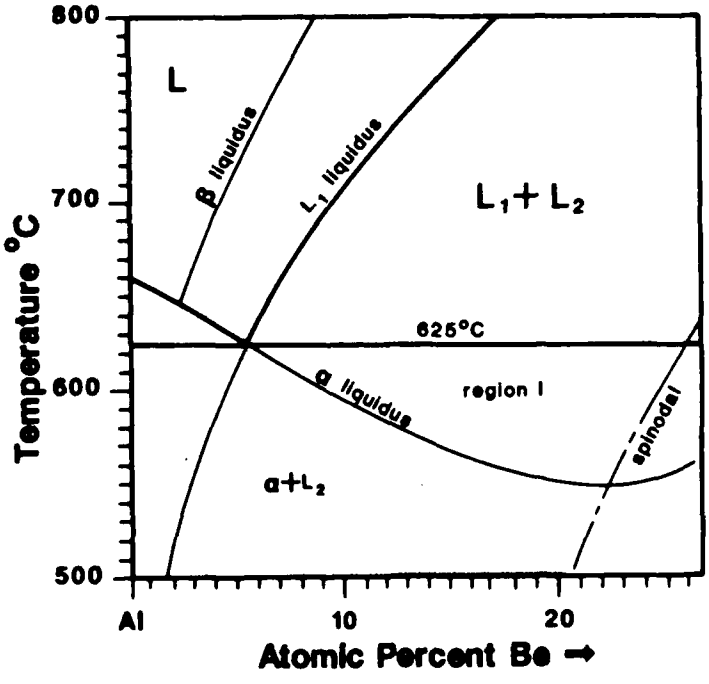

(b)

Fig.18. Metastable phase diagrams for the Al-Be binary system.

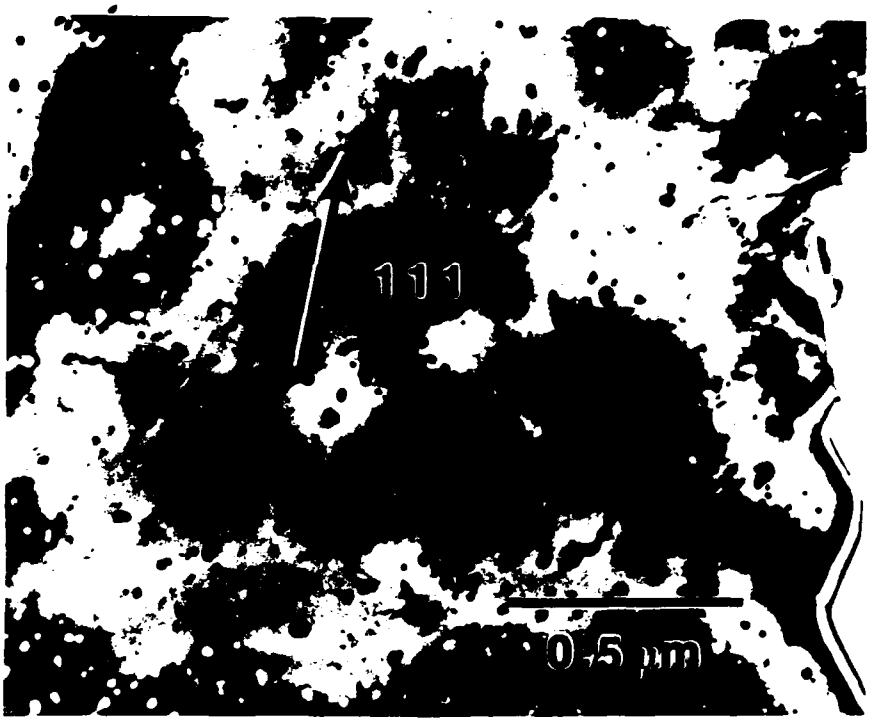

Fig.19. Transmission electron micrograph of melt-spun Al-4.4Be. The area is recorded from a transparent region of the ribbon, corresponding to very high rates of cooling.

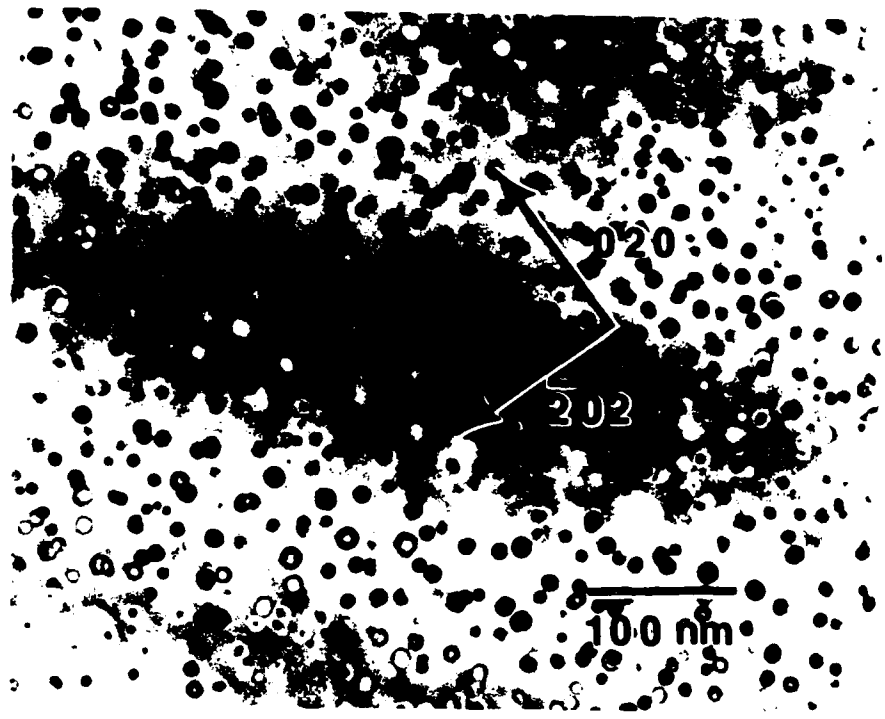

(a)

(b)

Fig.20. Transmission electron micrographs of an Al-Be alloy processed by LSR. a) An Al-5.8Be alloy showing microstructure produced by cooperative growth; b) An Al-11Be alloy showing microstructure produced by cooperative growth.

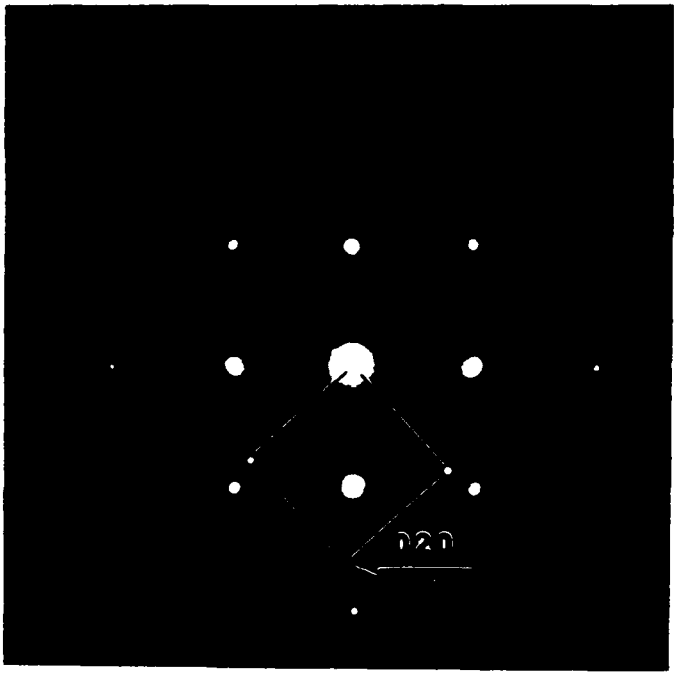

(a)

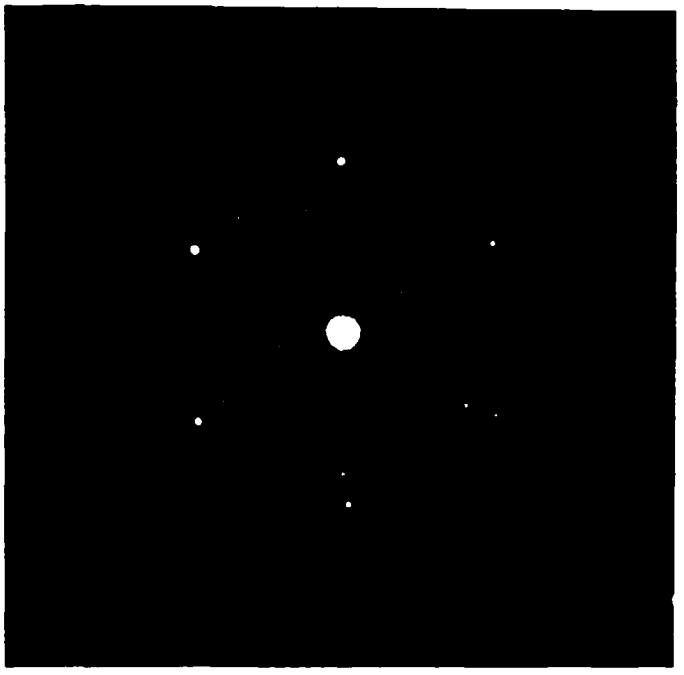

(b)

Fig.21. Convergent electron beam diffraction patterns of the Be-rich particles observed in the Al-11Be LSR filaments. The two patterns shown were obtained from two different Be particles in the same Al grain. The diffraction results indicate an equivalent crystallographic orientation between the Be particle and the Al matrix. (a) 100 zone axis with the $(010)_{Be}$ // $(010)_{Al}$ (b) 111 zone axes with $(100)_{Be}$ // $(110)_{Al}$.

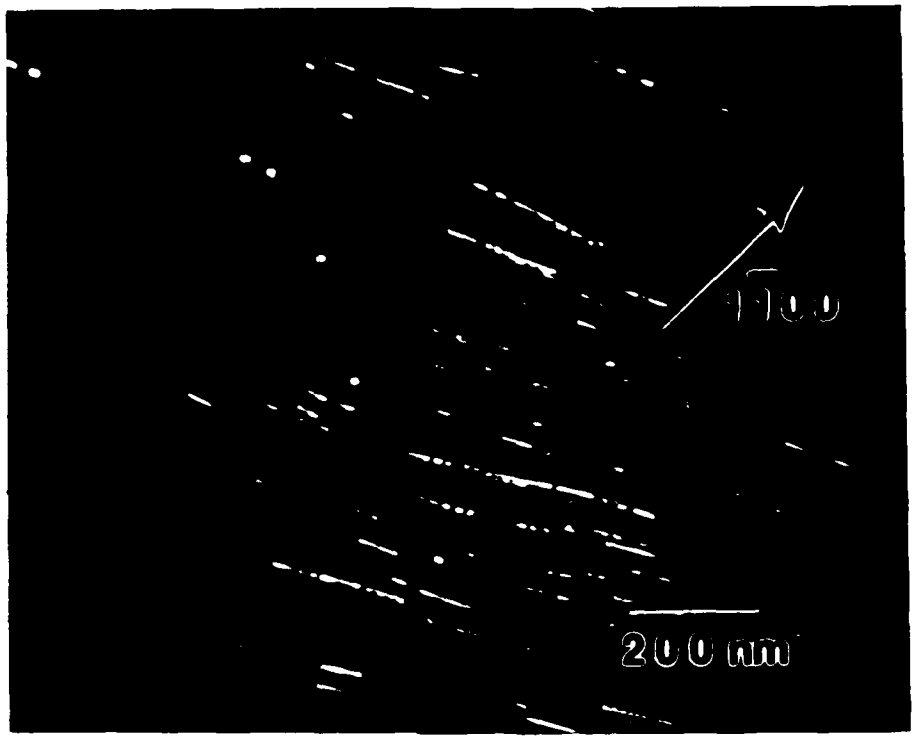

(a)

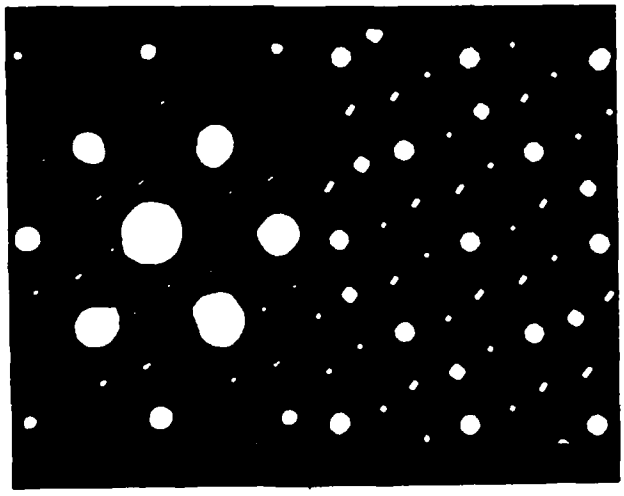

(b)

Fig.22. (a) TEM-DF. A rod morphology observed near regions of unmelted substrate observed in the Al-11Be alloy processed by LSR. (b) Experimental and computed electron diffraction patterns for the rod morphology. Calculations were based on orientation relationship #9 with $[101]_{Al}$ // $[0001]_{Be}$ with $(111)_{Al}$ // $(1210)_{Be}$.

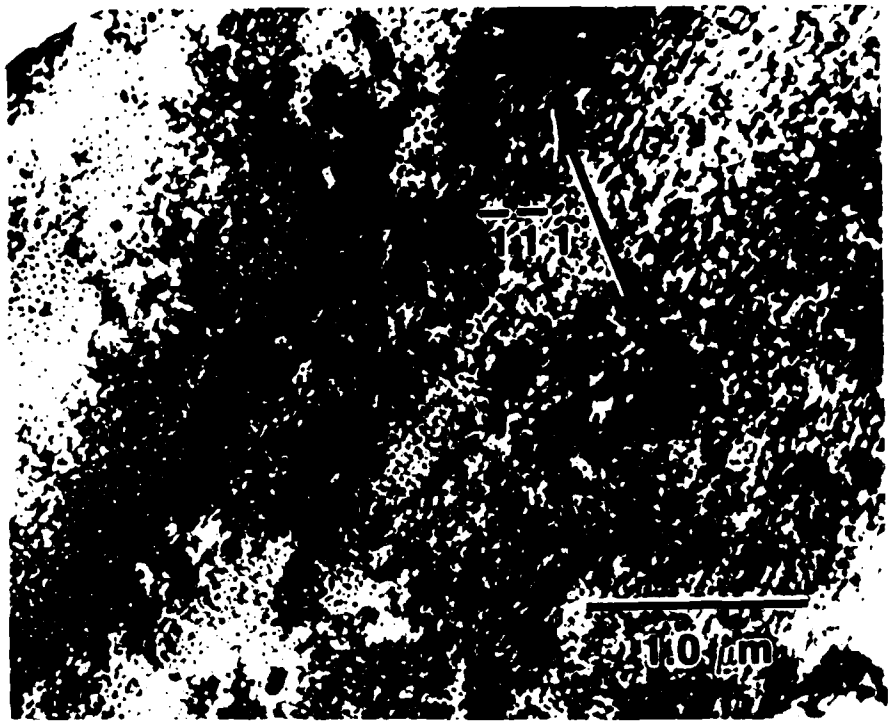

(a)

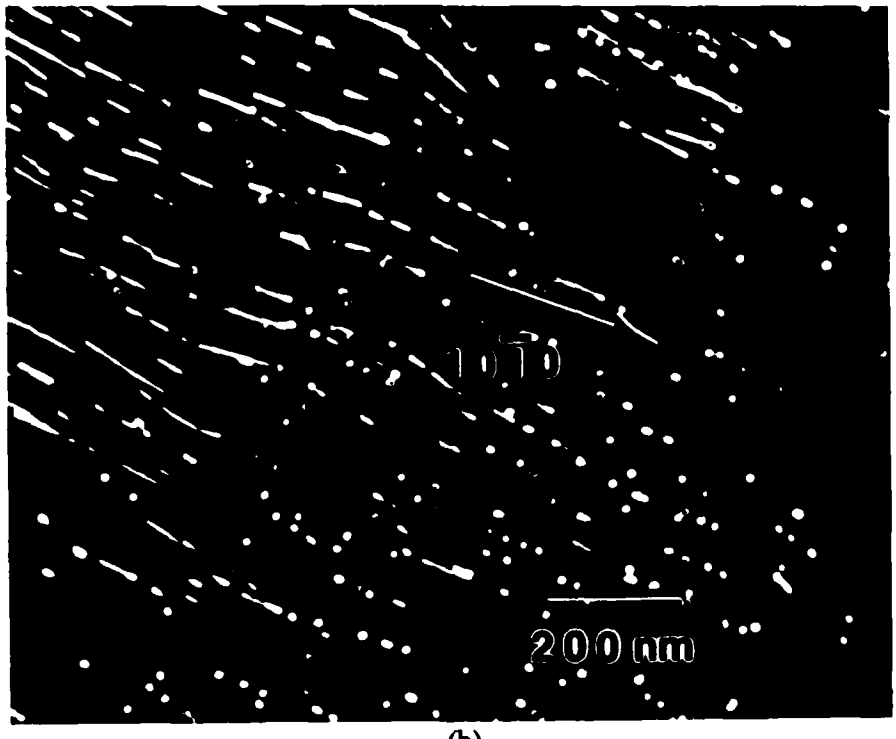

(b)

Fig.23. (a) TEM-BF. A single grain exhibiting the transition from the rod to a spherical dispersion. Top right to bottom left. (b) TEM-DF. A dark-field image showing the morphological break-down of the rod structure. An equivalent crystal orientation is suggested by the intensity observed in the rods and the smaller spherical powders.

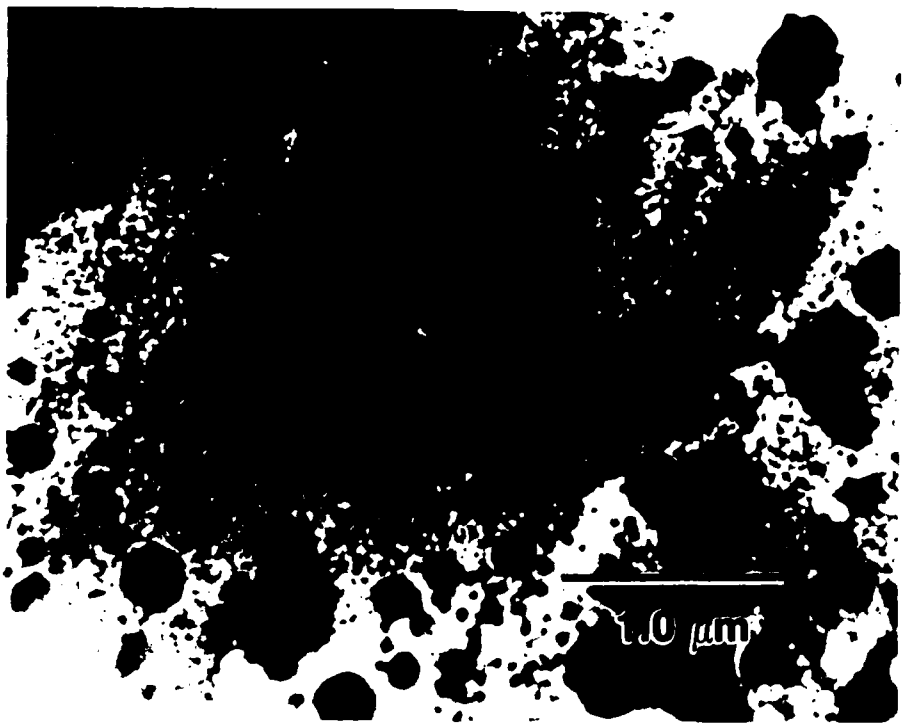

Fig.24. TEM-BF. An unpolished Al-7.3In alloy ribbon showing the presence of large In-rich particles in the microstructure.

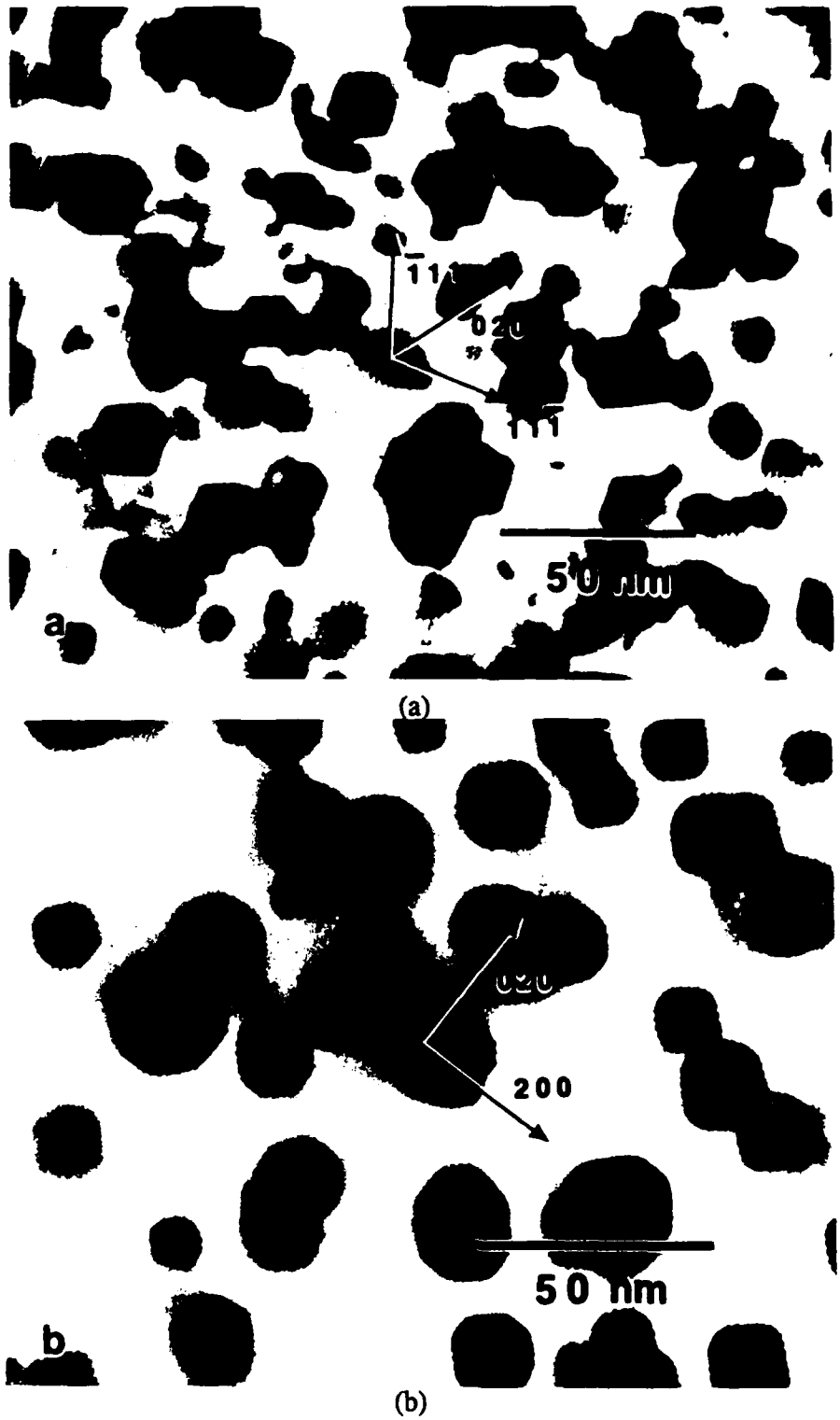

Fig.25. TEM. (a) A bright-field image recorded with the electron beam aligned parallel with a <101> Al crystal direction. The Moiré fringe pattern shows that the facets are parallel to {111} and {010} Al planes. (b) A bright-field image recorded with the electron beam aligned parallel with a <100> Al crystal direction. The Moiré fringe pattern shows that the facets are parallel to {010} and {011) Al planes. The {011} facets have been interpreted as the projected image of the {111} facets.

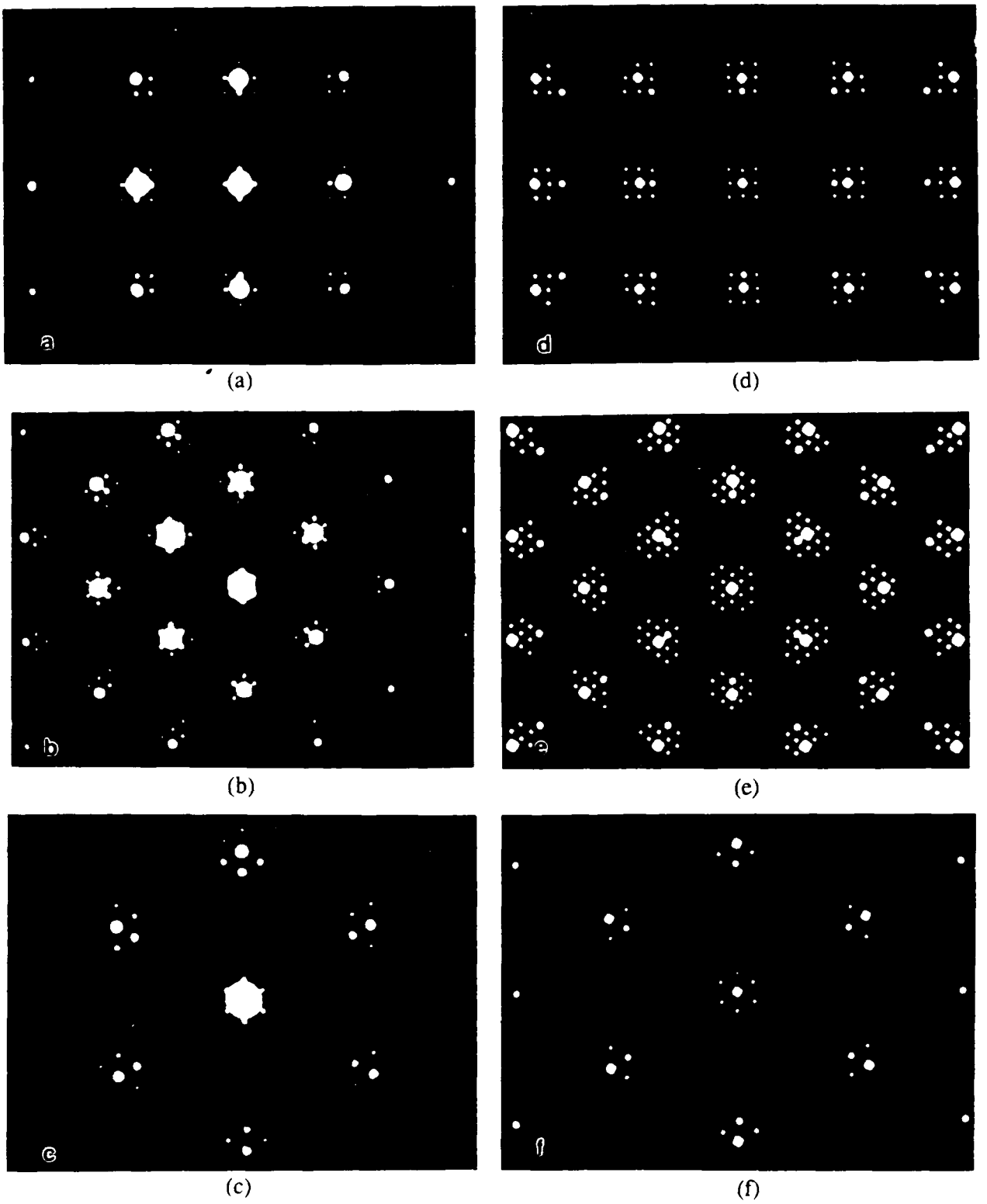

Fig.26. Selected area diffraction patterns recoreded from the small facetted In-rich particles. (a-c) Experimental diffraction patterns for [100], [101] and [111] zone axes of Al. (d-f) Calculated diffraction patterns for an Al matrix containing a In' particle with the following orientation relationship: $[100]_{Al}$ // $[100]_{In'}$ and $(010)_{Al}$ // $(010)_{In'}$. The large, medium and small computed diffraction spots are the matrix, precipitate and double diffraction spots, respectively.

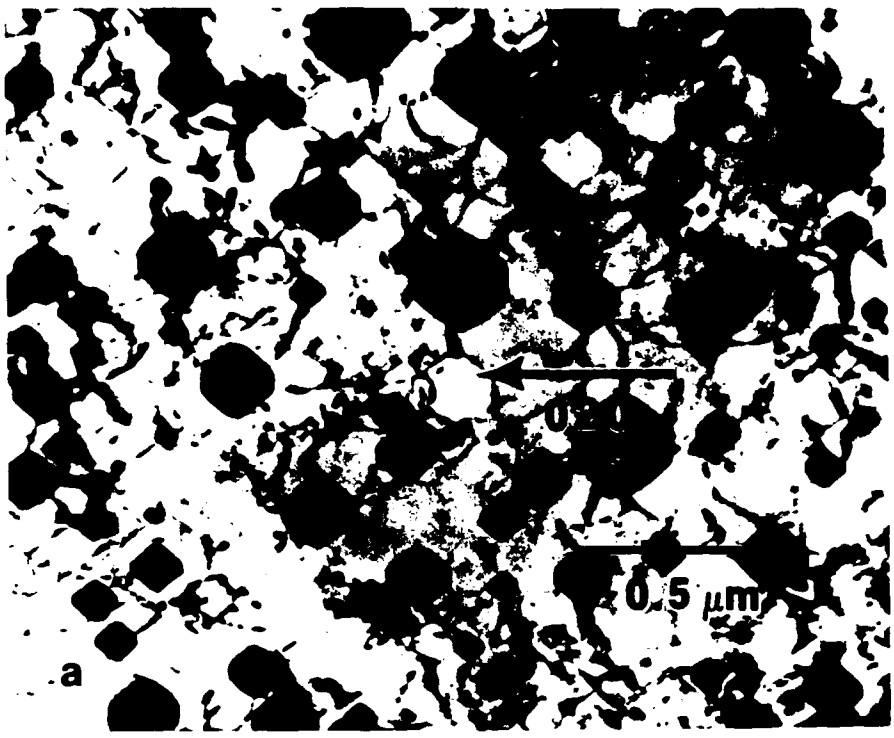

(a)

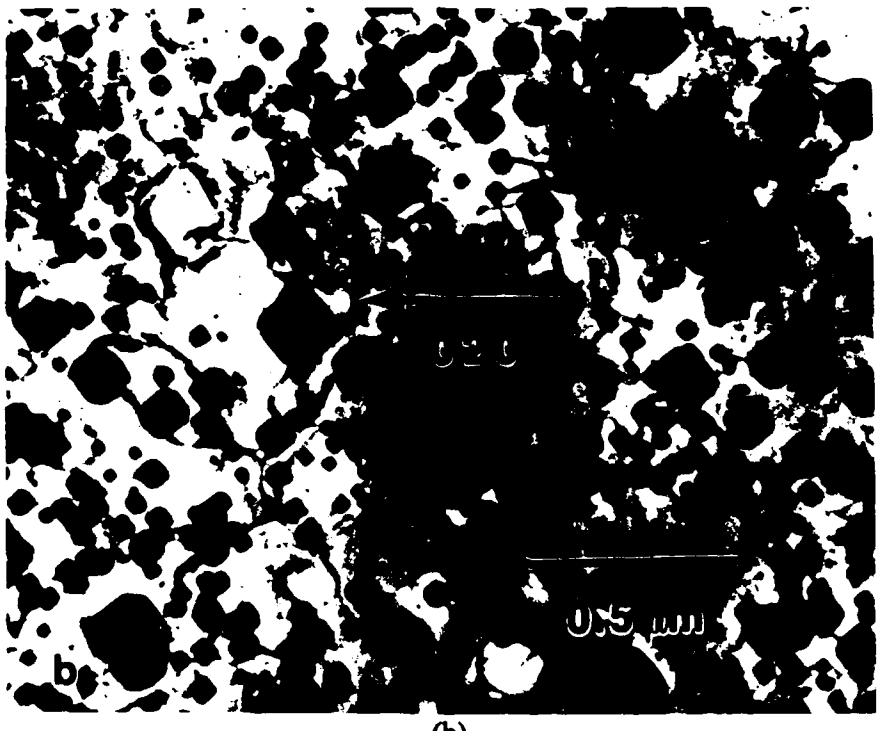

(b)

Fig.27. TEM-BF. Microstructures observed in ribbons thinned by ion milling. (a) Image recorded with the electron beam aligned parallel to a <100> Al axis. (b) Image recorded with the electron beam aligned parallel to a <100> Al axis.

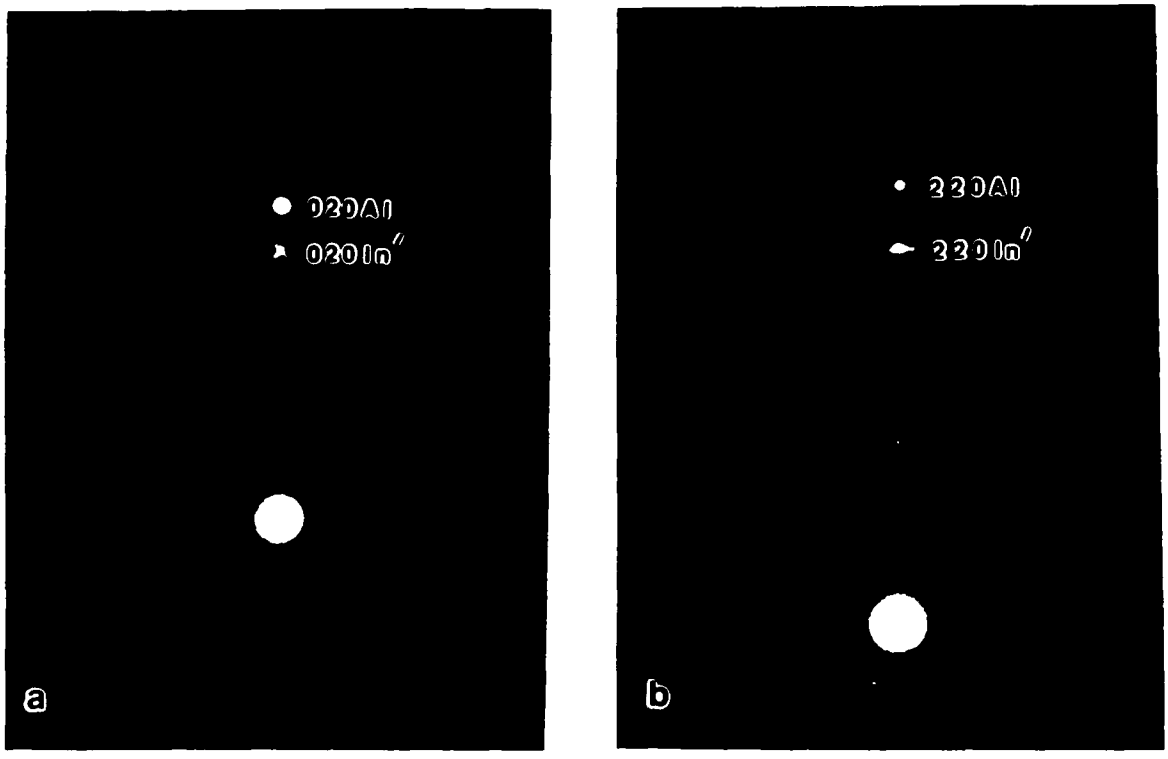

(a) (b)

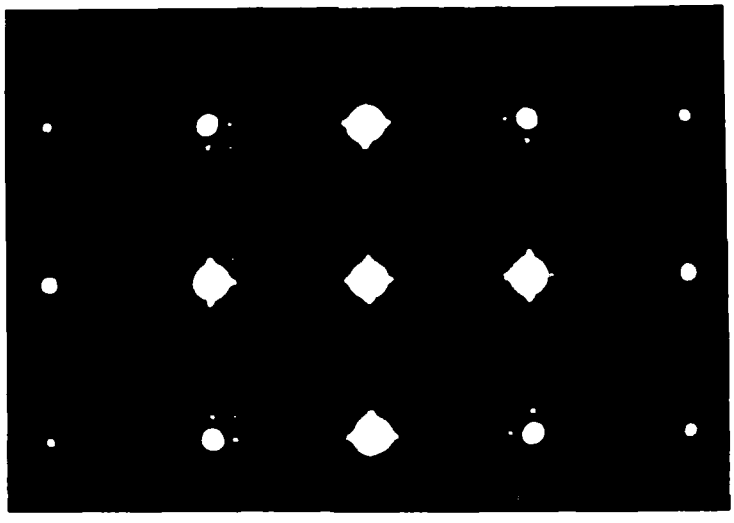

(c)

Fig.28. Selected area diffraction results for the large In' particles which were observed in the ion milled ribbons. (a) Streaking of the In' intensity in the <110> directions. (b) Streaking of the In' intensity in the [110] direction. (c) SAD pattern with the electron beam aligned parallel to a <100> crystal direction.

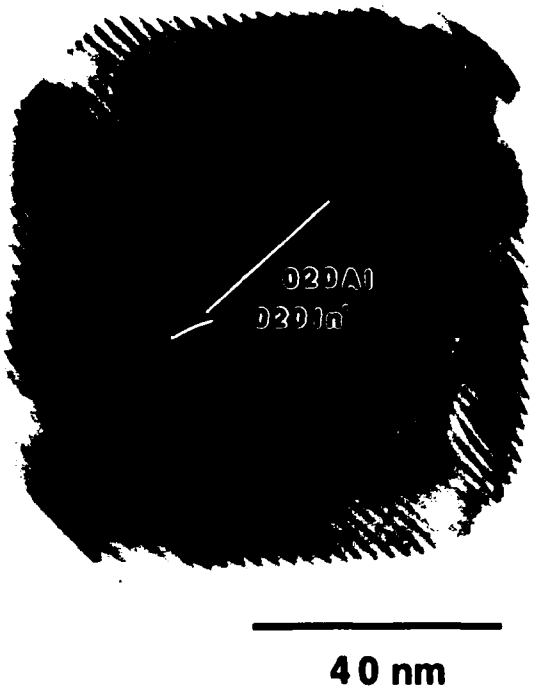

Fig.29. TEM-BF. A large In' particle showing Moiré fringe contrast. Note the twisting of the fringe pattern resulting from the trapped dislocations. The electron beam was parallel to a <100> crystal direction.

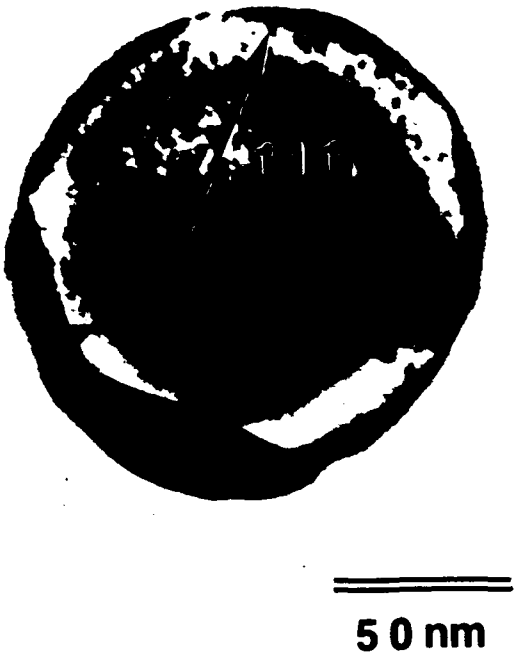

(a)

(b)

Fig.30. (a) TEM-BF. An EHD particle which shows the as-received microstructure and liquid phase separation. (b) Corresponding dark-field image shown with selected area diffraction results.

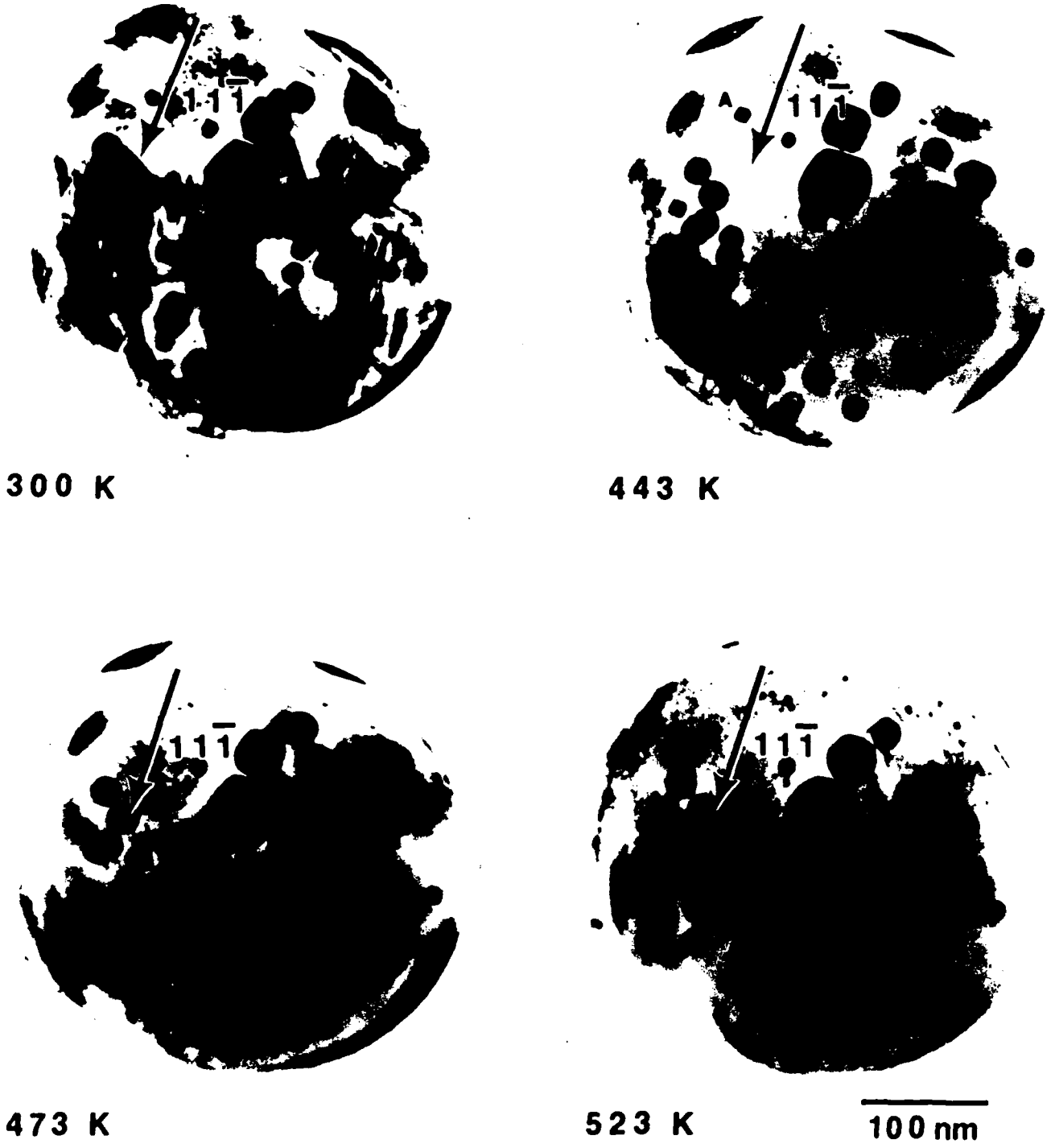

Fig.31. TEM-BF. A series of bright-field images recorded at elevated temperatures and with the electron beam aligned parallel to a <101> crystal direction to observe the facetting as a function of temperature.

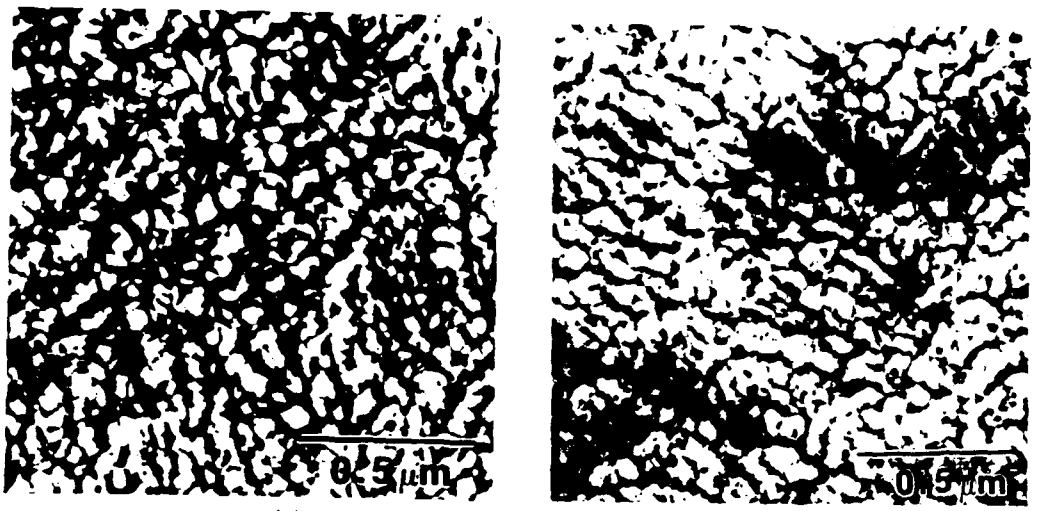

(a) (b)

Fig.32. Transmission electron micrographs showing typical microstructures for rapidly solidified (a) Al-Fe-Mo and (b) Al-Fe-Ce alloys.

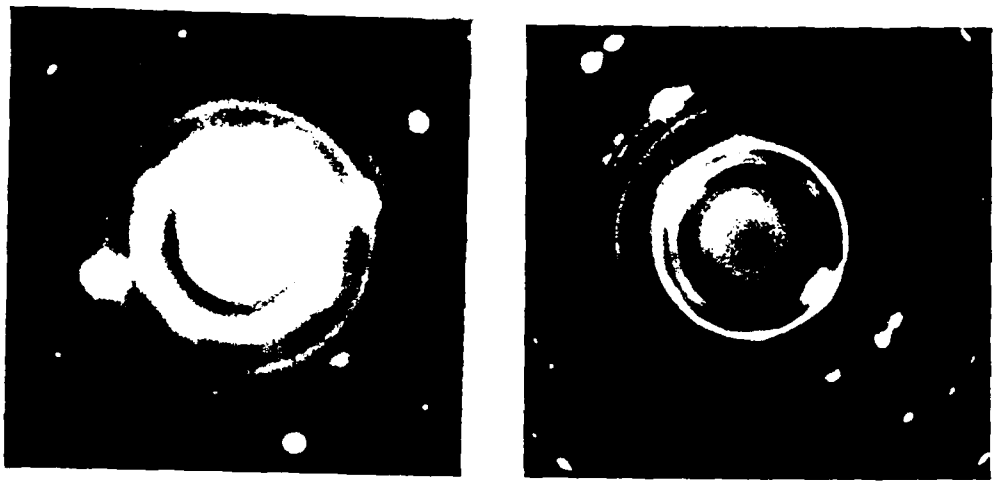

(a) (b)

Fig .33. Selected area diffraction patterns corresponding to the micrographs shown in Fig. 32; (a) Al-8Fe-2Mo and (b) Al-7.9Fe-2.9Ce

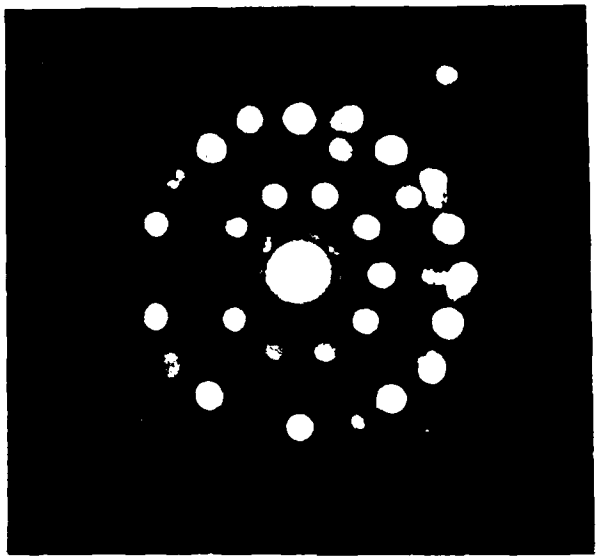

Fig.34. Convergent beam electron diffraction pattern taken from an individual intercellular particle in the Al-7.9Fe-2.9Ce alloy.

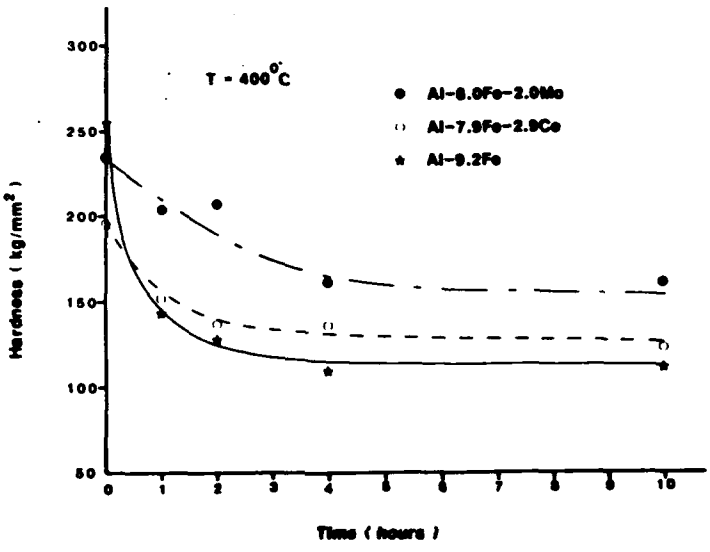

Fig.35. Results of micro-hardness measurements corresponding to isochronal annealing at 400°C of the alloys indicated.

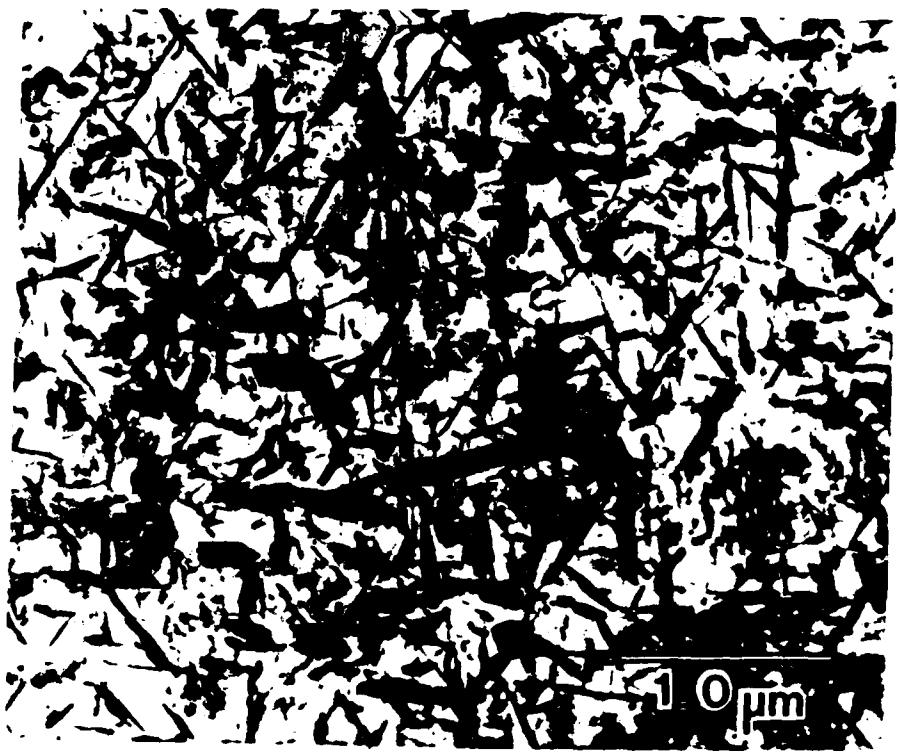

Fig.36. Transmission electron micrograph of decomposed microstructure of melt-spun Al-9.2Fe binary alloy following an anneal of four hours at 400°C.

4. CONSOLIDATION OF PARTICULATE

Most techniques for the consolidation of particulate involve the application of a combination of pressure and an extensive exposure to elevated temperatures. In the case of rapidly solidified materials this thermal excursion offers the possibility of microstructural decomposition and coarsening, which would be expected to have a detrimental effect on properties. For this reason, the thermal stability of the rapidly solidified product must firstly be assessed. For the sake of simplicity and interest, the following discussion will be limited to the alloy Al-8Fe-2Mo. The microstructures of the alloy before and after four hours at 400°C are shown in Fig.37a and b, respectively. As can be seen, the microstructure following annealing is more or less unchanged and this is consistent with only a small decrease in hardness, Fig.35. Presumably, this decrease in hardness is caused by the decomposition of the supersaturated α-Al solid solutions, effected by diffusion of the solute to the intercellular regions. This is at first an encouraging result since extrusion may be carried out at somewhat lower temperatures, i.e. in the range 300-400°C. For this reason, extrusion has been effected at 300°C, at an extrusion ratio of 14:1. During preparation of the material for extrusion, the particulate (chopped ribbon) was vacuum degassed at 325°C for approximately one hour.

The microstructure of the extruded material is shown in Fig.38. As can be seen, the zone A microstructure has decomposed and been replaced by one of an equiaxed nature. Two types of particles are present, one usually associated with the grain (or sub-grain) boundaries, the other having a needle-like morphology. The former type of precipitate appears to be the metastable Al_6Fe, while the needle-like phase is Al_3Fe. The reason for this decomposition of microstructure is of interest, particularly in view of the remarkable stability exhibited during annealing (e.g. Fig.37). From work involving annealing under the application of stress [38], it appears that the temperature during extrusion was increased to ≥450°C by adiabatic heating. Since the ram speed was chosen to be (approximately) as slow as possible (7.6mm.s^{-1}), and also since the extrusion ratio cannot be reduced much below the value used because it is necessary to rupture the residual oxide layers on the surfaces of the particulate, it seems that such adiabatic heating is unavoidable.

It seems that it is not possible to effect consolidation of melt-spun ribbons of the alloy Al-8Fe-2Mo using extrusion without inducing microstructural decomposition. Therefore, it is important to develop alternative methods of compaction which do not make use of prolonged thermal excursions. One such technique is dynamic compaction; a light weight projectile, accelerated to a velocity typically in the range 1000-3000m.s^{-1} by either compressed He (gas gun) or electromagnetically (rail gun), is caused to be incident on the particulate. Consolidation is thought to occur by the following mechanism. The shock wave caused by the impact of the

projectile on the target is transmitted through the particulate; the friction generated by the relative motion of adjacent particles causes local surface melting. Since the dwell time of the shock pulse is very short, these molten regions are rapidly solidified by the relatively cool powder interiors. In this way, compaction is effected without the bulk of the particulate experiencing elevated temperatures. A light-gas gun for dynamic compaction has been developed at the University of Illinois [39], the device being shown schematically in Fig.39. The microstructures of dynamically compacted ribbons of Al-8Fe-2Mo are shown in Fig.40; the velocity of the projectile was $\approx 1100 m.s^{-1}$ and essentially theoretical density has been achieved. Much of the microstructure is similar to that shown in Fig.40a; as can be seen both from the image and the diffraction pattern, there has been little, or no microstructural modification. In some areas there is evidence of decomposition, leading to the production of refined equiaxed grains (≈200nm in diameter), Fig.40b. Presumably, these areas correspond to the heat-affected regions, in the vicinity of prior ribbon boundaries. It appears that dynamic compaction may be used to consolidate zone A microstructures without causing significant microstructural decomposition. However, the mechanical properties of the compacts are not good, since essentially zero ductility is exhibited during mechanical property determinations.

(a)

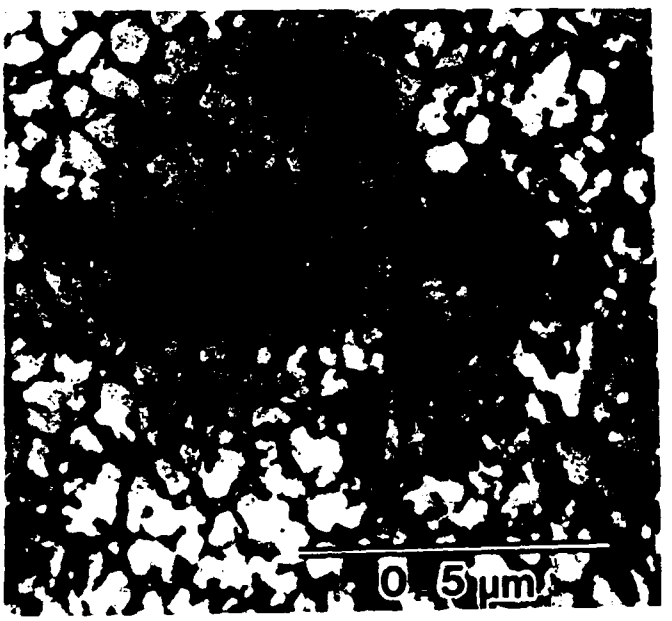

(b)

Fig.37. Microstructures of melt-spun Al-8Fe-2Mo alloy before (a) and after (b) annealing at 400°C for four hours.

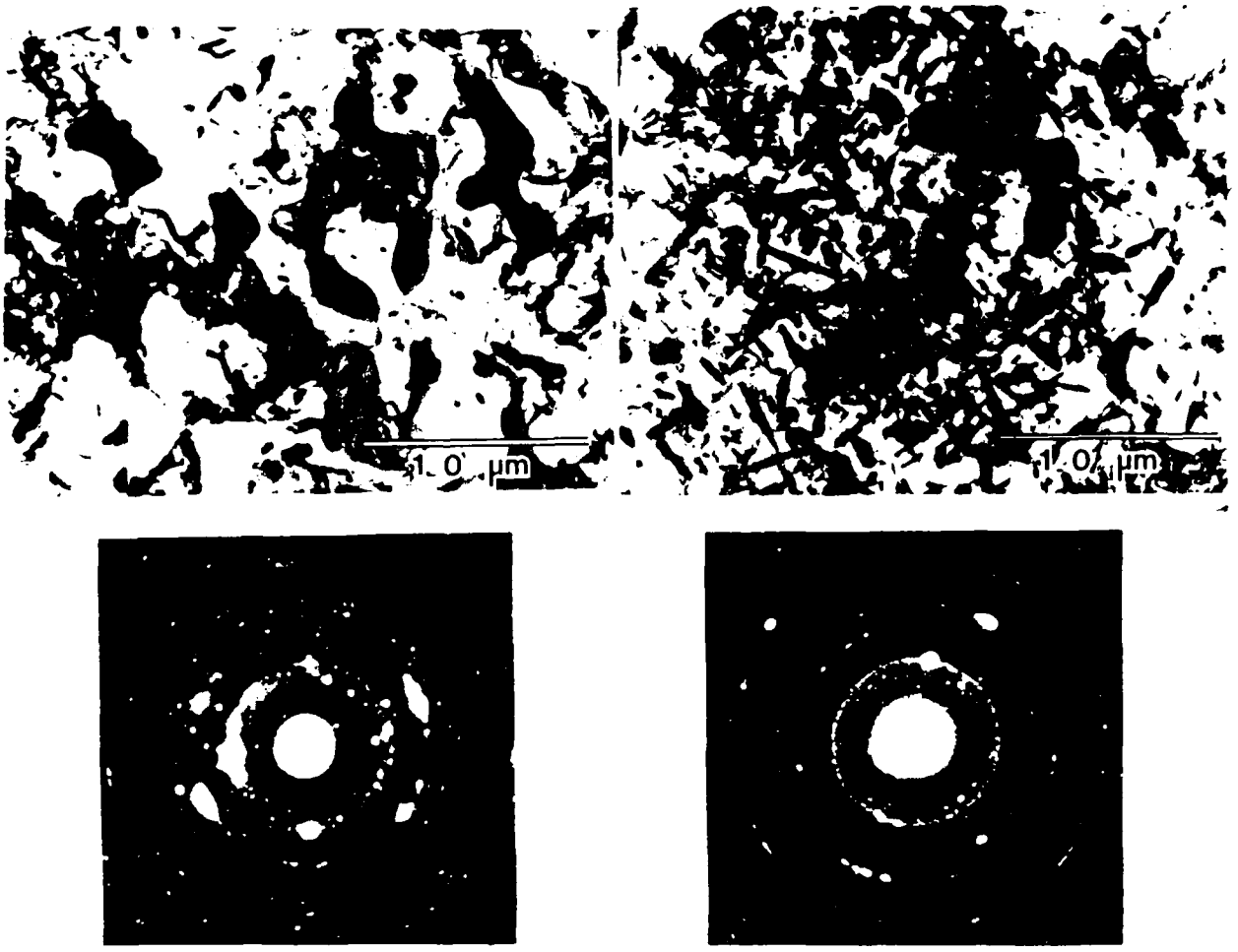

Fig.38. Transmission electron micrographs of extruded Al-8Fe-2Mo ribbons. See text for details.

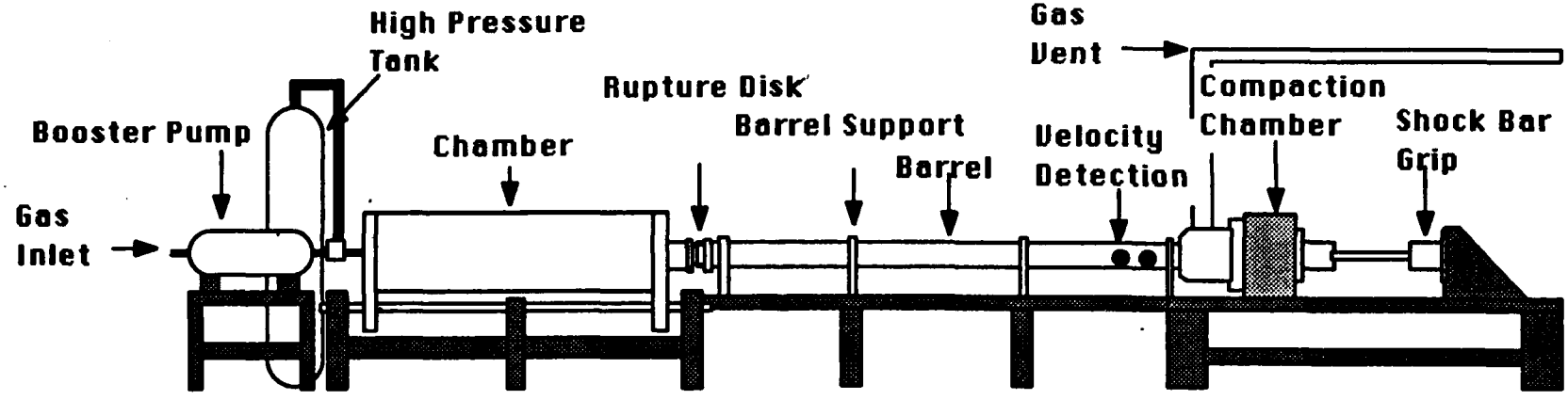

Fig.39. Schematic diagram of the dynamic compaction device.

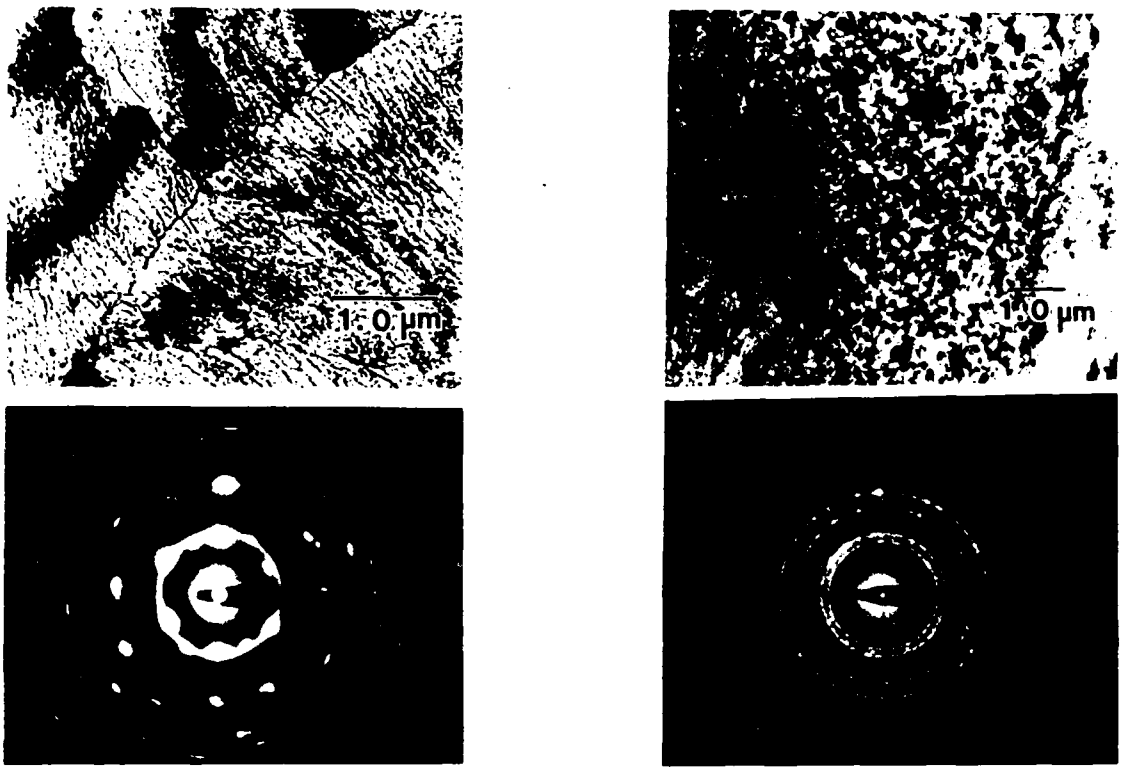

(a) (b)

Fig.40. Transmission electron micrographs of microstructures of dynamically compacted Al-8Fe-2Mo rapidly solidified powders; a) zone A material; b) evidence of some decomposition.

5. MECHANICAL PROPERTIES

5.1 Al-Fe Alloys

The work on mechanical properties of rapidly solidified alloys based on the Al-Fe system has concentrated on the alloy Al-8Fe-2Mo. The tensile properties of both extruded and laser surface melted samples have been determined. In addition, the fracture toughness of the extruded alloy has been assessed. These results will be described in turn.

5.1.1 Extruded Material

The results of monotonic tensile tests performed on samples machined from the extruded Al-8Fe-2Mo are shown in Table 3 [40]. These results may be compared with those obtained from extruded *RSR* powder [41]. Fig.41 shows a plot of the ultimate tensile strengths of the two types of material. Of course, these results are obtained from material with a decomposed microstructure.

Test Temp. (°C)	Young's Modulus (GPa)	Yield Strength (MPa)	Tensile Strength (MPa)	Reduction in Area (%)
20	82.0	404	462	4.0
315	63.4	239	282	32.5

Table 2. Results of tensile tests performed on extruded ribbon of Al-8Fe-2Mo tested at 20°C and 315°C.

5.1.2 Laser Surface Melted Material

In order to assess the strength of the same alloy (Al-8Fe-2Mo) with the zone A microstructure, small-scale tensile samples were machined from laser surface melted samples. Laser surface melting (3.5-4.5kW, 3mm diameter beam and traverse speed of 8.5cm.s^{-1}) in the case of this alloy results in a melted zone of cross-section approximately 0.25mm (depth) by 1.0mm (width) whose microstructure is entirely zone A. Tensile specimens were carefully machined, the geometry being given in detail elsewhere [42]. A photograph of a sample tested at room temperature is shown in Fig.42; the laser affected region is clearly visible, and it can be seen that the gauge section consists only of the zone A microstructure. It has been assessed that no significant stress concentrations are introduced because of the specimen geometry [43]. However, to

establish confidence in the results of these sub-scale tests, a sample of alloy 6061 in the T4 condition was fabricated and tested. The tensile strength of this sample was found to be ≈250MPa, which is similar to that recorded for a standard sized sample. In this way, it was concluded that the

Alloy	Fracture Stress (MPa)	Temperature (°C)
6061-T4	250	20
Al-8Fe-2Mo	520	20
Al-8Fe-2Mo	401	315

Table 3. Sub-scale tensile test results for 6061-T4 and laser surface melted Al-8Fe-2Mo at the temperatures indicated.

sub-scale tests would give rise to significant results. The results are given in Table 4. These results indicate that the laser surface melted (zone A) samples are considerably stronger than those of the extruded material. It is interesting to note that the laser surface melted samples exhibited essentially no ductility; this is due mainly to the presence of solidification defects in these samples. In fact, ribbons of this alloy which possess the zone A microstructure may be repeatedly bent through 180°, implying a ductility of at least ≈5% (at room temperature).

5.1.3 **Fracture Toughness - Extruded Material**

The fracture toughness of the extruded material was determined by the use of chevron-notched, short-rod specimens. The tests were valid with respect to plane strain (ASTM criteria being exceeded). The results are shown in Table 5, where values for 7075-T6511, 7178-T6511 and Al-8Fe-2Mo fabricated by extrusion of *RSR* powders (from Pratt and Whitney Aircraft (PWA)) are included for comparison. As can be seen, the values of the fracture toughness for the Al-8Fe-2Mo alloy are rather low, and unacceptable regarding commercial application. These low values may be due to two contributing factors. Firslty, the problems associated with the adherent oxide layers on Al alloy particulate may be responsible. Secondly, the morphology of the second phase may also cause a poor response in fracture toughness tests. Thus, the needle-like shapes of the Al_6Fe precipitates (Fig.38) would tend to give rise to stress-concentrations, resulting in lower values of toughness. It has recently been reported by Das [44] that the addition of a small amount of Si to these alloys causes the fracture toughness to increase to ≈27MPa$\sqrt{m}$; this is apparently due to the more attractive morphology of the decomposed microstructure. An example of the microstructure of melt-spun Al-8Fe-2Mo-1Si following an anneal of four hours at 450°C is given in Fig.43. As can be seen, the particles may be described as faceted, but considerably more spherical

than those found in the Si-free alloys. It appears then that morphology of the microstructure plays a very important rôle in the fracture toughness (and presumably fatigue properties) of these materials. Further work on this aspect is in progress.

Alloy	Specimen Orientation	Fracture Toughness (MPa $\sqrt{m}$)
7075-T6511	T-L	22.8
7178-T6511	T-L	17.1
Al-8Fe-2Mo:		
RSR Powder	T-L	9.25
Ribbons	T-L	13.25

Table 4. Fracture toughness values for the alloys indicated.

5.2 Plastic Deformation of Al-Be Alloys

Some mechanical properties of rapidly solidified Al-3.7Be, making use of either dynamic compaction or extrusion for consolidation, have been determined. The microstructures of the dynamically compacted and extruded ribbons are shown in Figs. 44 and 45, respectively. The dynamically compacted material consists of a refined dispersion of Be particles, within an heavily dislocated matrix of α-Al. In contrast, the extruded material consists of a dynamically recrystallized structure with elongated Al grains containing a coarse dispersion of Be particles. The density of the dynamically compacted material appeared to be ≈ 98.9%. Since the ribbons were not effectively compacted during this process, it was possible only to perform compression tests on these samples. Even so, the samples delaminated during testing, permitting only the determination of the modulus and yield strength. These values are compared to those measured from chill-cast Al-23Be in Table 6.

Alloy	Yield Strength(Mpa)	Ultimate Strength(MPa)	Hardness(DPH)
Al-4Be dyn. comp.	250.0	---	107.0
Al-23Be chill-cast	120.0	180.0	54.0

Table 5. Mechanical Test Results for Dynamic Compaction Samples

In the case of the extruded material, the consolidated samples were theoretically dense. Therefore, it was possible to perform tensile tests on this material and the monotonic tensile properties so determined are listed in Table 7.

Young's Modulus	71.5 GPa
Yield Strength	126.0 MPa
Ultimate Tensile Strength	163.0 MPa
Reduction in Area	83.0 %
Strain Hardening Coefficient	0.094

Table 6. Monotonic tensile properties for extruded Al-3.7Be

As can be seen, the yield stress for the dynamically compacted samples greatly exceeds that for the extruded material; this is presumably due to both the refined distribution of particles and the very high dislocation density resulting from the action of the shock wave in the dynamically compacted samples. It is interesting to note that the rapidly solidified alloy containing 3.7Be exhibits approximately the same strength as that of the as-cast alloy containing 23Be.

It is of interest to determine the mechanism of hardening in these alloys. For example, the microstructure of deformed samples may be examined to determine whether the Be particles were bypassed (Orowan mechanism) or sheared (Friedel cutting). When this is done in the case of the extruded material, the dislocation debris present is such as to obscure any Orowan loops, thus inhibiting a unique determination of the strengthening mechanism. It is known from Fig.45 that the average particle size in the as-extruded samples is $\approx$ 55nm with an average interparticle spacing of 255nm. To establish whether looping or shearing of particles is occurring for different particle sizes, samples of Al-4Be which had been laser surface melted were deformed 5-10% by cold rolling either in the rapidly solidified condition or following heat-treatment at 500°C for one hour. The microstructures of these two types of sample are shown in Figs.46 and 47. The average particle sizes were 10nm and 200nm, respectively, for the rapidly solidified and heat-treated samples. Note that in the heat-treated samples, the particles were elongated. In the case of the rapidly solidified samples(Fig.46), there is no evidence for Orowan looping, and it is assumed that Friedel cutting has occurred. This is consistent with the particles being fairly weak. For the heat-treated samples (Fig.47) there appears to be Orowan looping occurring about the particles; here, the particles are large and fairly widely spaced so that such looping is not unexpected. It may be concluded that, regarding Friedel cutting and Orowan looping, the Be particles present only a weak barrier to dislocation motion.

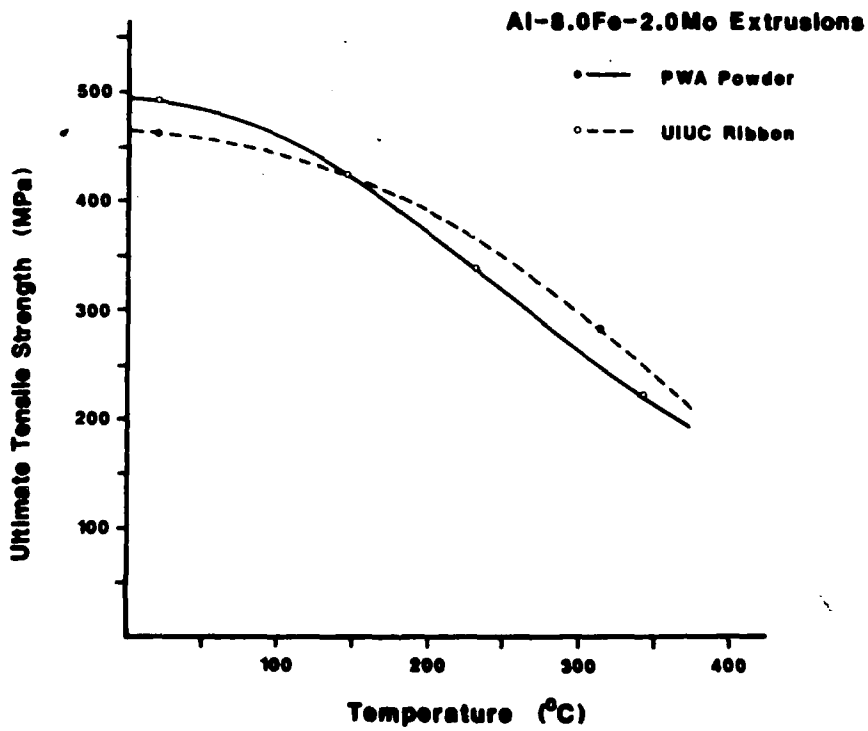

Fig.41. Plot of ultimate tensile strengths of the two alloys indicated.

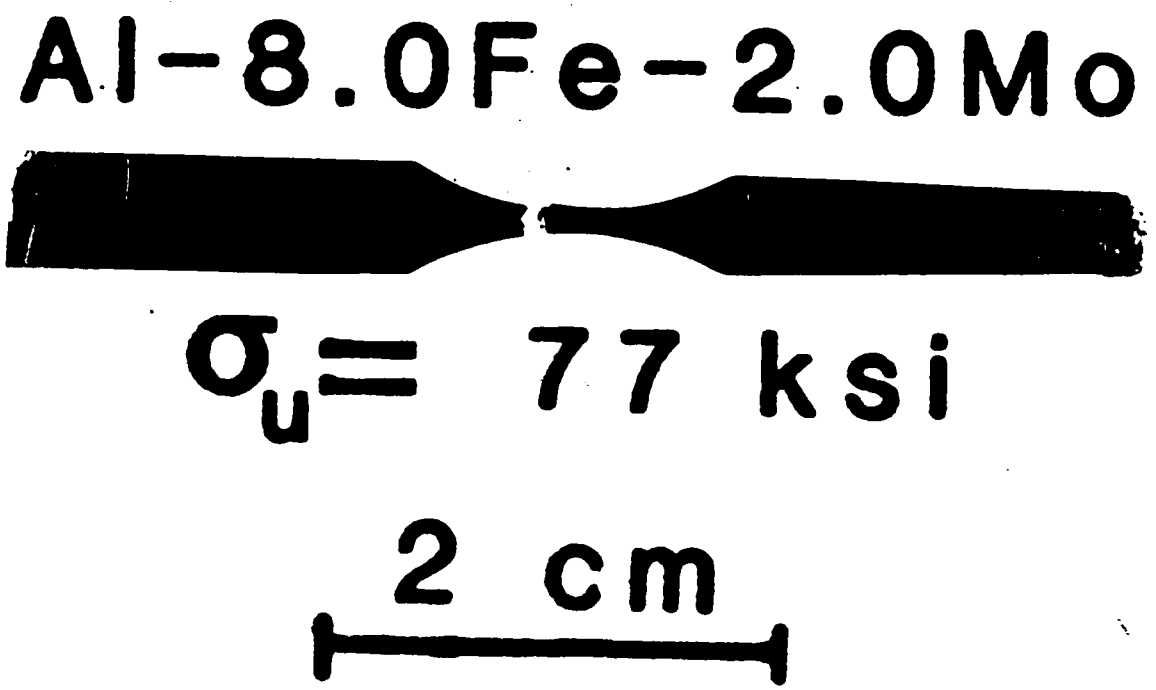

Fig.42. Photograph of laser surface melted tensile sample of Al-8Fe-2Mo tested at ≈20°C.

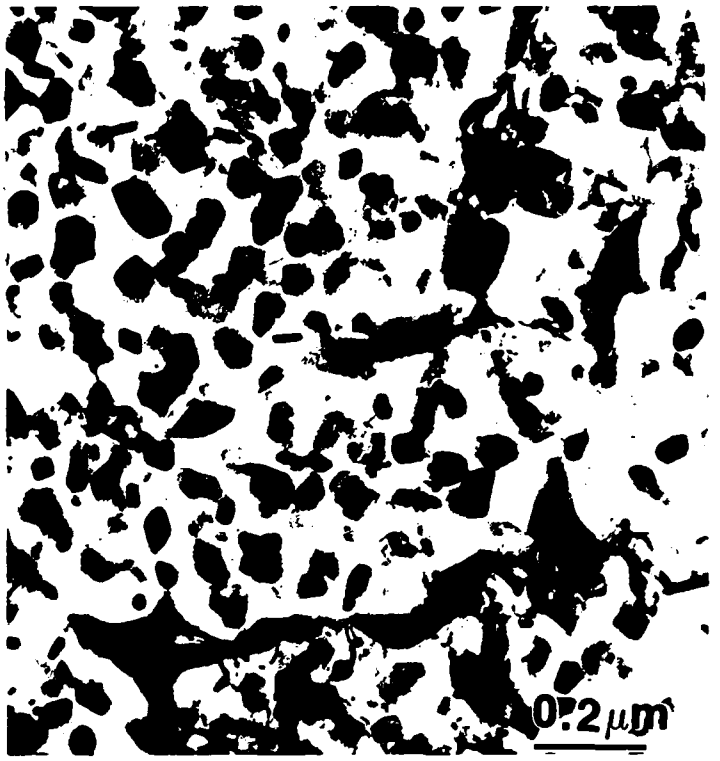

Fig.43. Transmission electron micrograph of melt-spun ribbons of Al-8Fe-2Mo-1Si following heat-treatment for four hours at 450°C.

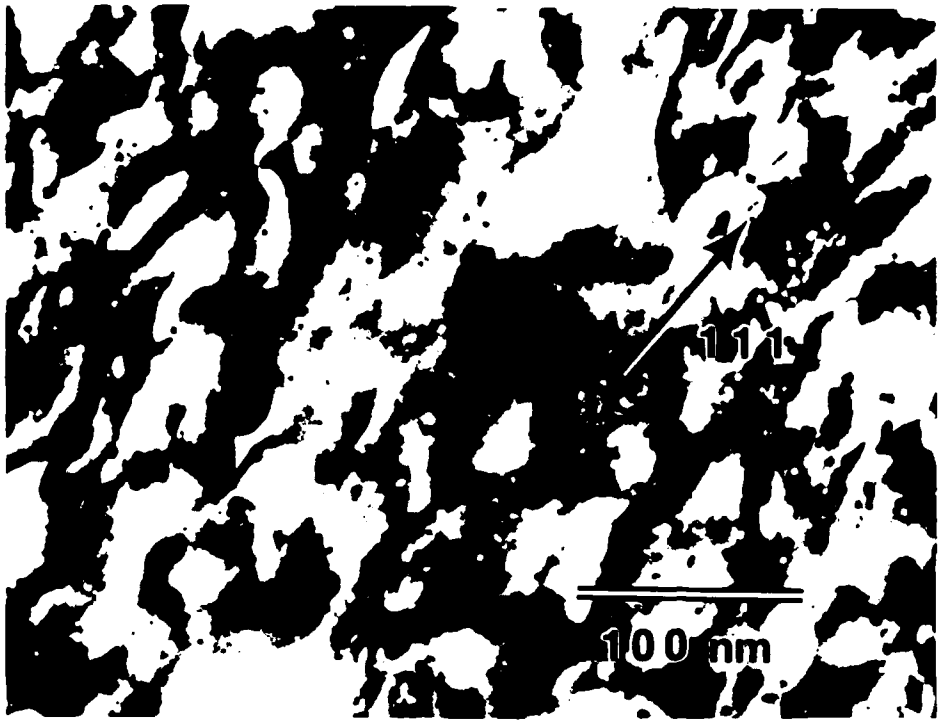

Fig.44. TEM-BF. Microstructures of the compacted ribbon. A high dislocation density was evident in the microstructure.

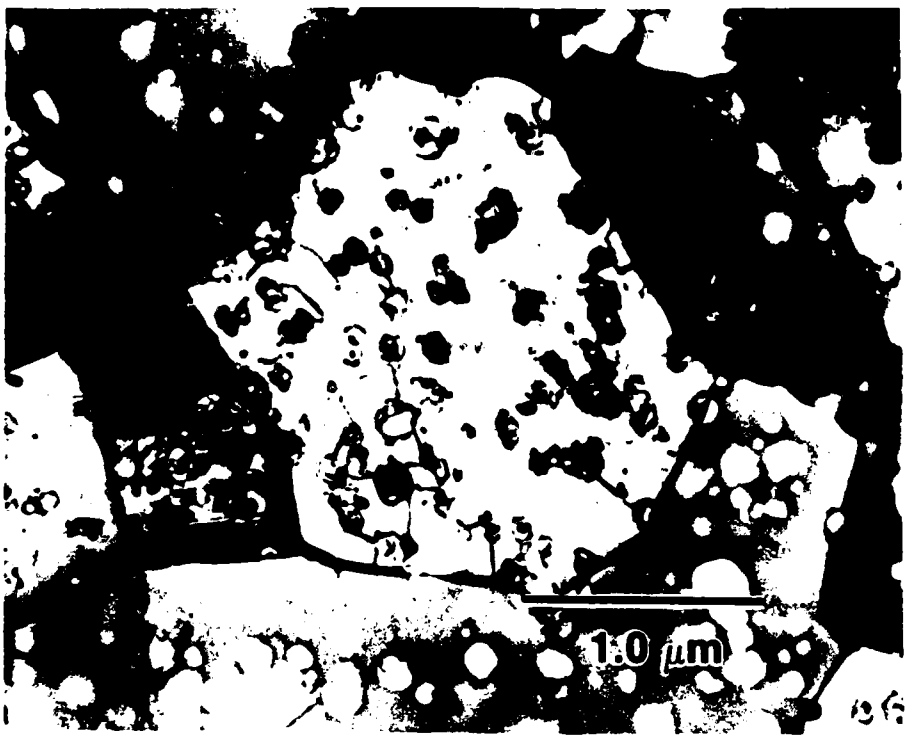

(a)

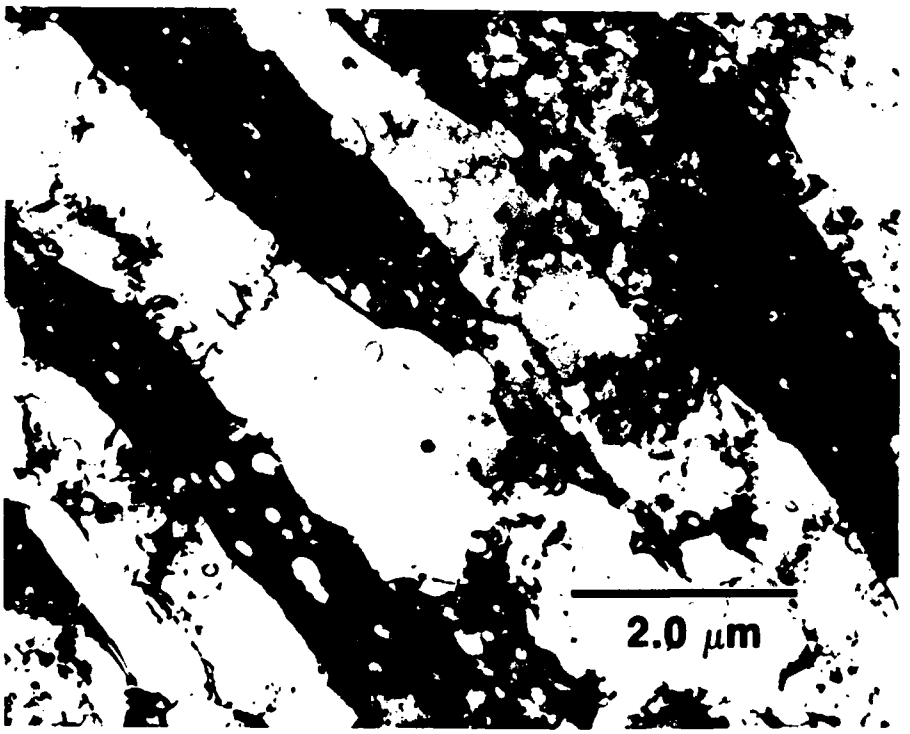

(b)

Fig.45. TEM. Bright-field electron micrographs from (a) transverse and (b) longitudinal cross-sections of the extruded Al-4Be ribbon.

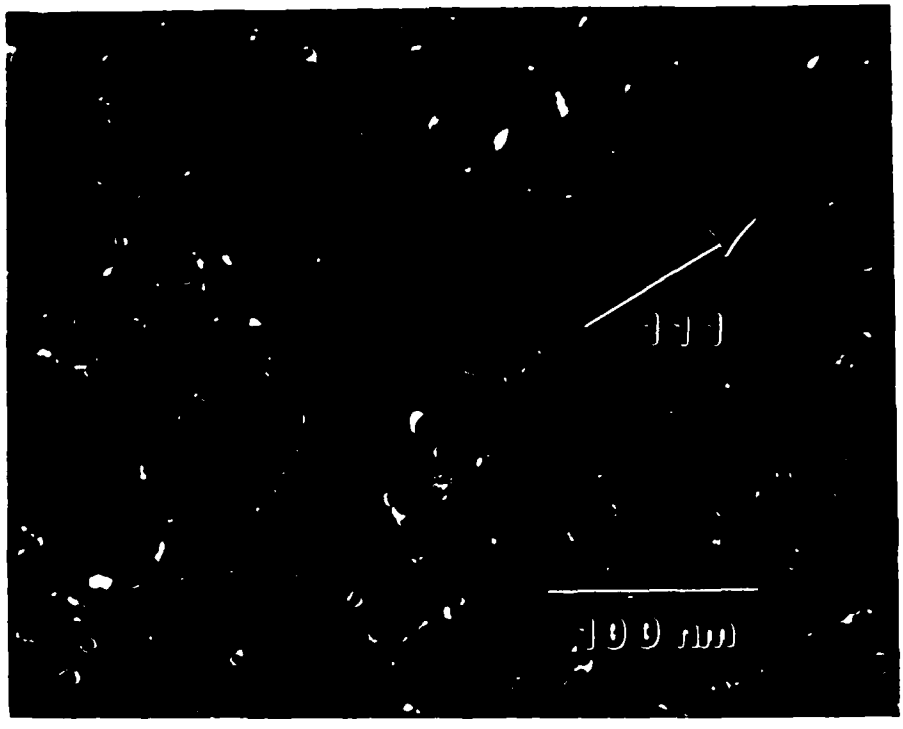

Fig.46. TEM. Weak-beam dark-field electron micrograph of the deformed LSM Al-4Be alloy. The absence of particle looping indicates a weak dislocation barrier and particle cutting.

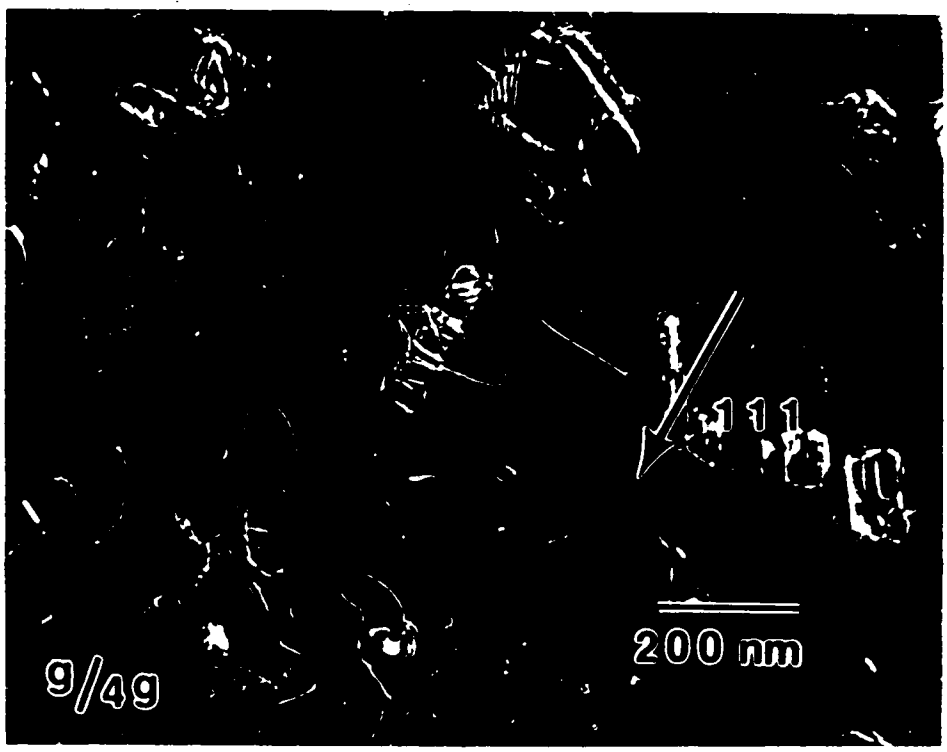

Fig.47. TEM. Weak-beam dark-field electron micrograph of the heat treated (1 hr. at 500°C) and deformed LSM Al-4Be alloy. Dislocations were observed to be looped around the central particle.

6. PUBLICATIONS FROM THIS PROGRAM

Microstructures of some Rapidly Solidified Al-based Alloys, D. C. VanAken, M. J. Kaufman, J. T. Stanley, R. D. Field and H. L. Fraser, in Proceedings of The Fifth International Conference on "Rapidly Quenched Metals", (S. Steeb, and H. Warlimont, eds.), Elsevier Science Publishers, p. 941, (1985).

The Microstructure of Rapidly Solidified Hypereutectic Al-Be Alloys, D. C. Van Aken and H. L. Fraser, Acta Met., 33, p. 963, (1985).

Mechanical Properties of Rapidly Solidified Al-Fe-X and Al-Be alloys, D. C. Van Aken, J. W. Zindel, R. D. Field, P. Kurath and H. L. Fraser, in "Mechanical Behavior of Rapidly Solidified Materials", (S. M. L. Sastry, and B. A. Macdonald, eds.), TMS-AIME, Warrendale, PA., p. 189, (1985).

Rapid Solidification and subsequent analysis of some Hypereutectic Al-base Alloys, J. W. Zindel, J. T. Stanley, R. D. Field and H. L. Fraser, "ASTM STP 890", (M. E. Fine, and E. A. Starke Jr. eds.), p. 186, (1985).

Dynamic Compaction of Rapidly Solidified Aluminun Alloy Powders, J. W. Sears, D. J. Miller and H. L. Fraser, "ASTM STP 890", (M. E. Fine, and E. A. Starke Jr. eds.), p. 304, (1985).

The Elastic Modulus Of Rapidly Solidified Al-Mn and Al-Be Alloys, D. C. Van Aken, D. J. Miller, P. Kurath and H. L. Fraser, in Proceedings of Symposium on "Aluminum Powder Metallurgy", TMS-AIME Fall Meeting, Toronto, Canada, p. 14-17, (1985).

Microstructure and Mechanical Properties of Al-8wt%Fe-2wt%Mo Melt Spun Ribbon, J. W. Zindel and H. L. Fraser, in Proceedings of Symposium on "Aluminum Powder Metallurgy", TMS-AIME Fall Meeting, Toronto, Canada, p. 18-23, (1985).

Microstructure and Properties of Rapidly Solidified Al-Fe (Mo/Ce) Alloys, J. W. Zindel, R. D. Field, P. Kurath and H. L. Fraser, in Proceedings of the International Conference "Aluminum Alloys, Their Physical and Mechanical Properties", (E. A. Starke Jr. and T. H. Sanders Jr. eds.), Chameleon Press Ltd, London, Vol. 1, p. 279, (1986).

Mechanical Properties of Rapidly Solidified Al-4Be alloys, D. C. Van Aken, P. Kurath and H. L. Fraser, in Proceedings of the International Conference "Aluminum Alloys, Their Physical and Mechanical Properties", (E. A. Starke Jr. and T. H. Sanders Jr. eds.), Chameleon Press Ltd, London, Vol. 1, p. 295, (1986).

The Formation of Microstructures in Rapidly Solidified Hypereutectic Al Alloys containing Ni or Co, J. T. Stanley, R. D. Field and H. L. Fraser, in Proceedings of the International Conference " Aluminum Alloys, Their Physical and Mechanical Properties", (E. A. Starke Jr. and T. H. Sanders Jr. eds.), Chameleon Press Ltd, London, Vol. 1, p. 307, (1986).

Rapid Solidification of Al Alloys, H.L. Fraser, in Proceedings of the International Conference " Aluminum Alloys, Their Physical and Mechanical Properties", (E. A. Starke Jr. and T. H. Sanders Jr. eds.), Chameleon Press Ltd, London, In Press, (1986).

Dynamic Compaction of Al Alloys, J.W. Sears, B.C. Muddle and H.L. Fraser, Mat. Res. Soc.

Symp. Proc. Vol 28, Elsevier Science Publishing Co., Inc., p. 163 (1984).

J.W. Zindel, J. T. Stanley, R. D. Field and H. L. Fraser, Mat. Res. Soc. Symp. Proc. Vol 28, Elsevier Science Publishing Co., Inc., p. 317, (1984).

The intercellular phase in Rapidly Solidified Alloys based on the Al-Fe system, R. D. Field, J. W. Zindel and H. L. Fraser, Scripta Met., 20, 415-418, (1986).

Precipitates in a Rapidly Solidified Al-Mn Alloy possessing Icosahedral Symmetry, R. D Field and H. L. Fraser, Mater. Sci. and Eng., 68, p. 117, (1984/85).

Nucleation in the presence of a Metastable liquid Miscibility gap in the Aluminum Beryllium system, D. C. Van Aken and H. L. Fraser, Hume-Rothery Memorial Symposium, TMS-AIME Spring Meeting, 1986, In Press.

Microstructural Comparison of Rapidly Solidified Al-base Powders Produced by Laser Surface Melting, Melt Spinning, and Atomization, J. W. Zindel, J. T. Stanley, R. D. Field and H. L. Fraser, in Proceedings of the "International Powder Metallurgy Conference", Toronto, Canada, June 17-22, 1984, In Press.

A Microstructural Comparison of Melt Spun and Laser Surface Melted Aluminum-Molybdenum Alloys, F. C. Grensing and H. L. Fraser, Met Trans. A, In Press.

The Mechanism of Formation of Microstructures in Rapidly Solidified Hyper-eutectic Al Alloys, J.T.Stanley, R.D.Field and H.L.Fraser, Acta Met., In Press.

Rapidly Solidified Al-In Alloys, D.C.Van Aken and H.L.Fraser, Int. J. of Rapid Solid., In Press.

Master Degree supported by program:

Rapid Solidification of Aluminium-Molybdenum; Fritz Carl Grensing

Doctor of Philosophy Degrees supported by program:

Microstructures and Properties of Rapid Solidified Aluminium Alloys;

Jacob Wesley Zindel

Al-Be Composites Produced by Rapid Solidification;

David Carlton Van Aken

Doctor of Philosopy Degree supported by program but not yet completed:

Consolidation of Rapidly Solidified Particulate; Dean J. Miller

7. REFERENCES

1. Lifshitz, I.M. and Slyozov, J.J., Phys. Chem. Solid. 19, 1961, 35
2. Predecki, P., Giessen, B.C. and Grant, N.J., Trans. TMS-AIME, 233, 1965, p.1438.
3. Jones, H., Mater. Sci. Eng., 5, 1969, p.1.
4. Jacobs. W.H., Doggett. A.G. and Stowell, M.J., Jnl. Mats. Sci., 9, 1974, p.1631.
5. Griffith, W.M., Kim, Y-W., Froes, F.H., "Powder Metallurgy Processing of Aluminum Alloy 7091," Rapidly Solidified Powder Aluminum Alloys, ASTM STP 890. Edited by M.E.Fine and E.A.Starke, Jr., American Society for Testing and Materials, Philadelphia, 1986, p.283-303.
6. Shechtman, D., Blech, I., Gratias, D. and Cahn, J.W., Phys. Rev. Lett., 53, No.20, Nov.12, 1984, p.1951.
7. Zindel, J.W., Stanley, J.T., Field, R.D., and Fraser, H.L., "Rapid Solidification and Subsequent Analysis of Some Hypereutectic Aluminum-Based Alloys," Rapidly Solidified Powder Aluminum Alloys, ASTM STP 890. Edited by M.E.Fine and E.A.Starke, Jr., American Society for Testing and Materials, Philadelphia, 1986, p.186-210.
8. Stanley, J.T., Field, R.D. and Fraser, H.L., "Aluminum Alloys: Their Physical and Mechanical Properties", E.A.Starke and T.H.Sanders, eds., Chameleon Press, London, 1986, pp.307.
9. Stanley J.T., Field, R.D. and Fraser, H.L., in preparation for submission to Met Trans.
10. Boettinger,W.J., "Rapidly Solidified Amorphous and Crystalline Alloys." Edited by B.H.Kear, B.C.Giessen, and M.Cohen, Elsevier Sci., New York, 1982, p.15.
11. Garrett, R.K. and Sanders, T.H., Matls. Sci. Eng. 60, 1983, p.269.
12. Kattamis, T.Z. and Flemings, M.C., Trans. AIME 236, 1966, p.1523
13. Kattamis, T.Z., and Mehrabian, R., J.Vac.Sci.Tech., 11 (6), 1074, p.1118
14. Levi, C., Ph.D. Thesis, Univ. of Illinois, 1981, p.30.
15. Van Aken, D.C. and Fraser, H.L., Acta Met., 33, 1985, p.963.
16. Marich, S. and Jaffrey, D., Met. Trans., 2, 1971, p.2681.
17. Perepezko, J.H. and Boettinger, W.J., MRS Symp. on Alloy Phase Diagrams. Edited by L.H.Bennet, T.B.Massalski and B.C.Giessen, Elsevier, North-Holland, 19, 1983, p.223.
18. Van Aken, D.C., Kurath, P. and Fraser, H.L., "Aluminum Alloys: Their Physical and Mechanical Properties", E.A.Starke and T.H.Sanders, eds., Chameleon Press, London, 1986, pp.295
19. Murray, J.L. and Kahan, D.J., Bull.Alloy Phase Dia., 4, 1983, p.50.
20. Tanner, L., private communication.
21. Ojha, S.N. and Chattopadhyay, K., Trans. Indian Inst. Metals, 31, 1978, p.208
22. Kaufman, M.J. and Fraser, H.L., Met. Trans.A, 14A, 1983, p.623.
23. Raynor, G.V. and Graham, J., J. Inst. of Metals, 84, (1955-56) p. 86
24. Betteridge, W., Proc. Phys. Soc., 50, 1938, p.519

25.Tyzack, C. and Raynor, G. V., Trans. Faraday Soc. 50, 1954, p.675

36.Guttman, L., TMS-AIME, 188, 1950, p.1472

27.Williams, C., Delavignette, P., Gevers, R. and Amelinckx, S., Phys. Stat. Sol., 17, 1966, K173

28.Poon, S.J., Drehman, A.J. and Lawless, K.R., Phys. Rev. Lett., 55, 1985, p.2324.

29.Ball, M.B. and Lioyd D.J., Scripta Met., 19, 1985, p.1065.

30.Bendersky, L., Schaefer, D.J., Biancaniello, F.S., Boettinger, W.J., Kaufman, M.J. and Shechtman, D., Scripta Met., 19, 1985, p.909.

31.Penrose, R. (a) Bull. Inst. Math. and its appl., 10,1974, p.266, (b) Math.Intell. 2,1979, p.32.

32.Socolar,D. and Steinhardt, P.J., private communication

33.Nelson, D.R., and Sachdev, S., Phys. Rev. B, 32, 1985, p.689.

34.Field, R.D. and Fraser, H.L., Mater. Sci. and Eng. 68, 1984/85, p.117.

35.Pauling, L., Nature,317, 1985, p.512.

36.Field, R.D., Zindel, J.W., and Fraser, H.L., Scripta Met., 20, 1986, p.415.

37.Urban, K., Moser, N. and Kronmuller H., to be published in Phys. Stat. Sol. (a).

38.Miller, D.J. and Fraser, H.L., in preparation for submission to Met. Trans.

39.Sears, J.W., Miller, D.J. and Fraser, H.L., "Dynamic Compaction of Rapidly Solidified Aluminum Alloy Powders," Rapidly Solidified Powder of Aluminum Alloys, ASTM STP 890. Edited by M.E.Fine and E.A.Starke, Jr., American Society for Testing and Materials, Philadelphia, 1986, p.304-318.

40.Zindel, J.W., Field, R.D., Kurath, P. and Fraser, H.L.,"Aluminum Alloys: Their Physical and Mechanical Properties", E.A.Starke and T.H.Sanders, eds., Chameleon Press, London, 1986, pp.288.

41.Adam, C.M., Bourdeau, R.G. and Broch, J.W., Application of Rapidly Solidified Alloys, AFWAL Final Report No. AFWAL- TR-81-4118, Feb.1982, Contract No.F33615-76-C-5136.

42.Zindel, J.W., Van Aken, D.C., Field, R.D., Kurath, P. and Fraser, H.L., TMS-AIME, New York, 1985, In Press.

43.Peterson, R.E., "Stress Concetration Factors". John Wiley & Sons, New York, 1974.

44.Das, S., Oral presentation, Westech '86 LA, CA.

END

1-87

DTIC